Title: Manganese and Soil Organic Carbon Stability on a Hawaiian Grassland Rainfall Gradient

Elizabeth L. Paulus*[1], Peter M. Vitousek[2]

[1]Geochemistry and Biogeochemistry Group, SLAC National Accelerator Laboratory, Menlo Park, California 94025 USA; [2]Stanford University Department of Earth System Science, Yang and Yamazaki Environment and Energy Bldg 140, 437 Via Ortega, Stanford, California 94305 USA

*Corresponding author: paulus@stanford.edu

Author contributions: Both authors designed the study and conducted the fieldwork. ELP conducted the laboratory analyses, analyzed the data, and wrote the article with contributions from PMV.

Keywords: manganese, organic carbon, grassland, manganese peroxidase, redox cycling

Abstract

Manganese (Mn) is a possibly critical yet poorly understood element controlling soil carbon (C) stocks. In temperate forests, Mn availability correlates strongly with organic C decay, but we know little about its role in soil organic matter decomposition in most terrestrial environments. In this study, we evaluate Mn in grassland C dynamics along a rainfall gradient in Hawaii. We measured Mn, organic matter, and microbial enzyme activities along the rainfall gradient to evaluate relationships among Mn oxidation state, chemical/biological reactivity, and soil C turnover. Neither Mn abundance nor its oxidation state are strong predictors of organic C instability along the grassland gradient. We also used an incubation experiment to investigate how dissolved organic C and CO_2 release from the grassland soil respond to increased Mn bioavailability. We found that Mn availability did not correlate with soil C instability; Mn additions corresponded with lower dissolved organic C and CO_2 fluxes from soils than did additions of deionized water. Mn availability may not predict soil C stability as well as previously thought.

1. Introduction

Manganese (Mn) is a reactive, biologically essential element ubiquitous in soil. It composes 0.1% of the Earth's crust (Turekian and Wedepohl, 1961), is the most energetically favorable redox-active metal, and has been shown to interact with soil organic matter (SOM) (Cui and Dolphin, 1990; Berg and McClaugherty, 2003; Berg et al., 2007; Davey et al., 2007; Keiluweit et al., 2015; Whalen et al., 2018), the largest reservoir of potentially dynamic carbon (C) on Earth (Ciais and Sabine, 2013; Köchy et al., 2015). Yet Mn remains one of the least understood elements influencing soil C stocks.

Mn exists in three oxidation states in soils: Mn^{2+} is the most reduced, energetically stable, soluble species and the only nutritionally available form; Mn^{3+}, a powerful and unstable oxidant, is the most reactive form (van der Lee, 1999; Rezanezhad et al., 2014; Keiluweit et al., 2016; Jones et al., 2018); and Mn^{4+}, which can also act as an oxidant, is the most oxidized and least soluble form. Mn cycles through these dynamic states when soil redox conditions fluctuate. Mn^{2+} is the most common form in primary minerals; it is released to soils through weathering and can be oxidized in the presence of O_2 to Mn^{3+}. Mn^{3+} can persist if stabilized in mineral forms or combined with ligands; otherwise, it is further oxidized to Mn^{4+} or reduced back to Mn^{2+} (Madden and Hochella, 2005; Webb et al., 2005; Lan et al., 2017). Where soils are anoxic, Mn^{4+} can be reduced to Mn^{2+} (Schulze et al., 1995), with Mn^{3+} as a possible, albeit thermodynamically unlikely, intermediate product (Luther, 2005). The forms of Mn and how Mn functions in soils depend on the soils' micro- and macroenvironments.

As organic matter (OM) breaks down, Mn accumulates. A comprehensive literature review found Mn concentration highly correlated with degree of decomposition, appearing to be "the single main factor" predicting OM decay in many study sites (Berg et al., 2010). Oxic-anoxic interfaces are ubiquitous within soils and have been found to be hotspots of Mn^{2+} oxidation (Mn^{3+} production), soil organic matter (SOM) oxidation, and microbial activity (Rezanezhad et al., 2014; Jost et al., 2015; Jones et al., 2018). Due to its small size, solubility, and potent reactivity, Mn^{3+} is the oxidation state directly involved in SOM breakdown: when chelated, most commonly in soils by a low-molecular-weight organic acid (LMWOA) (e.g., citrate), Mn^{3+} can persist long enough to diffuse into complex soil matrices and non-specifically oxidize previously protected OM, breaking the compound down into now accessible constituents (Janusz et al., 2013; Whalen et al.,

2018). Understanding what governs Mn^{3+} production in soils will clarify its role in destabilizing SOM.

Although, Mn^{4+} reduction and Mn^{2+} oxidation can ultimately enhance SOM breakdown by generating Mn^{3+}, Mn^{2+} oxidation is the primary route directly generating Mn^{3+}. Oxidation can occur abiotically or biotically. Abiotic oxidations are highly redox and pH sensitive (Jung et al., 2017; Zhang et al., 2021); biotic Mn oxidation depends less on pH and may progress more rapidly than abiotic oxidation in most natural systems (Hastings and Emerson, 1986; Tebo et al., 2004; Villalobos et al., 2006; Luther, 2010; Learman et al., 2011; Santelli et al., 2011). Microbes are, accordingly, thought to be the primary driver of Mn oxidation in natural environments (Emerson et al., 1982; Tebo et al., 1984; Tebo and Emerson, 1985; Clement et al., 2009; Dick et al., 2009). While diverse taxa (bacterial, archaeal, and fungal) living in many different environments can oxidize Mn (Hansel and Learman, 2016), evidence suggests fungi are the major biotic catalysts in soils (Possinger et al., 2022).

SOM derives from decomposed plant tissue, and its stability varies with a soil's microenvironment—mineral composition; structure; texture; water content; and microbial community, activity, and distribution (Meentemeyer, 1978; Gramss, 1997; Paul, 2006; Schmidt et al., 2011; Cotrufo et al., 2013; Lehmann and Kleber, 2015; Heckman et al., 2021; Possinger et al., 2022). In laboratory experiments, low O_2 availability limits OM mineralization by inhibiting white-rot fungi, which are aerobic decomposers (Kirk and Farrell, 1987); but in the field, OM degradation is greatest when O_2 fluctuates and in microsites near anoxic-oxic interfaces (Hall et al., 2015; Jones et al., 2018). Of the litter-degrading fungi, white-rot fungi are the most efficient decomposers (Abbas et al., 2005; Wong, 2009; Dashtban et al., 2010). They include numerous basidiomycetes species and a few ascomycetes, characterized by the suite of extracellular enzymes

86 they can secrete: phenol oxidases (laccase), heme peroxidases (e.g., lignin peroxidase [LiP] and
87 Mn peroxidase [MnP]), and versatile peroxidase (VP) (Martínez et al., 2009; Sigoillot et al., 2012).
88 Other fungi produce laccases, but the peroxidases are a hallmark of white rot (Riley et al., 2014).
89 Not all white rot fungi make LiP and VP, but all known species produce MnP (Hofrichter, 2002),
90 suggesting that MnP plays a conserved role in their metabolism (Hatakka and Hammel, 2011;
91 Floudas et al., 2012). Despite their name, ligninolytic enzymes attack a variety of SOM
92 biopolymers, not just lignin (Cui and Dolphin, 1990; Baldrian, 2006).

93 To degrade SOM's polymers and phenolic constituents, oxidative enzymes must be small
94 and non-specific themselves or use small, nonspecific reactive mediators to diffuse into structures
95 and attack diverse bonds (Hatakka and Hammel, 2011). When stabilized by weak ligands, Mn^{3+}
96 can serve as a reactive mediator. All the discussed enzymes (MnP and VP directly; laccases, VP,
97 and LiP indirectly) can oxidize Mn^{2+} to generate Mn^{3+}. MnP, though, should be the main actor, for
98 it is the most common and more potent than VP and laccases (Hofrichter, 2002; Hatakka and
99 Hammel, 2011). In some systems (e.g, temperate forests), MnP represents up to 99% of
100 ligninolytic-enzyme expression (Entwistle et al., 2018). It is also the only enzyme dependent on
101 Mn^{2+}, which serves as its sole reducing substrate and increases its expression and activity
102 (Paszczyński et al., 1986; Brown et al., 1991; Li et al., 1995; Sigoillot et al., 2012). In contrast,
103 Mn availability does not affect laccase and VP expressions and may even inhibit LiP production
104 (Janusz et al., 2013). Therefore, MnP appears to be the enzyme most clearly tied to Mn and its
105 influence on OM degradation.

106 The distribution of Mn in soil profiles depends on a network of factors. Like other cations,
107 Mn can be pumped through biological uplift from subsurface to surface soils and leached within
108 or from soils (Hernandez-Soriano et al., 2012). Soil E_h, pH, and SOM concentration, which

influence Mn speciation, vary throughout soil profiles and often on a microscale (Keiluweit et al., 2018; Wanzek et al., 2018). Mn concentrations and oxidation states in soils evolve from complex interactions among the relative intensities of biological uplift, leaching, pH, and redox conditions. Above ground, in temperate and tropical forests, the influence of Mn on OM decomposition dynamics (decomposition rate and the mix of compounds ultimately transferred to SOM) has been clearly demonstrated (Berg et al., 2007, 2010; Davey et al., 2007; Keiluweit et al., 2015; Trum et al., 2015; Fujii et al., 2020). No such study exists on grasslands. OM stability depends on the ecosystem, hinging on complex interactions among the abiotic and biotic factors of an environment (Schmidt et al., 2011; Lehmann and Kleber, 2015). An ecosystem's climate, potential organo-mineral interactions, nutrient accessibility, and plant and microbial community and functioning influence OM decomposition. Given the differences between temperate forests and grasslands, Mn may not exercise the same control on grass-litter decomposition as it reportedly does on forest-litter decay.

In this study, we investigate if Mn significantly influences soil organic C (SOC) turnover in a grassland by evaluating Mn redox cycling, Mn oxidation states, dissolved organic C (DOC), and CO_2 efflux in soils along the Kohala rainfall gradient. We hypothesize that if Mn is a dominant controller of SOC stability, patterns in Mn^{3+} redox cycling and Mn^{4+} abundance (the two oxidizing Mn species) should correlate with DOC concentration and CO_2 efflux. We also use an incubation experiment to investigate whether supplemental bioavailable Mn^{2+} has the same destabilizing effect on OC in a grassland soil as it does in temperate forests (Berg et al., 2007, 2010; Davey et al., 2007; Keiluweit et al., 2015; Trum et al., 2015). To our knowledge, this is the first study to evaluate how Mn directly affects SOM in a grassland. This work elucidates Mn redox cycling in field soils and investigates its influence on grassland SOM.

2. Materials and Methods

2.1 Study Sites

This study uses a grassland rainfall gradient to decipher the role of Mn in soil C cycling. The field sites are arrayed along a ~14-km transect on Kohala Mountain, Island of Hawai‘i (Figure 1). This is a well-characterized rainfall gradient that receives <300 to >3200 mm mean annual precipitation (MAP) (Giambelluca et al., 2013): mean annual temperatures and elevation range from 23.5˚C and 50 m at the driest site to 16˚C and 1000 m at the wettest site (Giambelluca et al., 2014). It has been thoroughly studied for decades. Most germane to this study, Chadwick et al. (2003) developed an integrated analysis of weathering and pedogenesis, Vitousek and Chadwick (2013) identified pedogenic thresholds and process domains, Peay et al. (2017) surveyed microbial community compositions, and von Sperber et al. (2017) evaluated N cycling on the gradient (Chadwick et al., 2003; Vitousek and Chadwick, 2013; Peay et al., 2017; von Sperber et al., 2017).

All sample points are located on the same ~150,000-year-old Hawī volcanic formation (Chadwick et al., 2003; Sherrod et al., 2007), possess the same relief, and have been grazed by cattle for over 100 years (Kagawa and Vitousek, 2012). Soils are volcanic Andisols: Typic Haplotorrands in the driest sites and Typic (or Hydric) Fulvudands in the wettest sites (Chadwick et al., 2003). The gradient also offers multiple advantages specific to understanding Mn-SOM interactions: sites span an expansive range of rainfall, soil pH (Figure S1A), soil water content (Figure S1B), soil redox conditions (Figure S1C), and SOM (Figure 4A) while parent material, topography, and vegetation remain consistent.

2.2 Field Study: Sample Collection

155 Grass (*Pennisetum clandestinum* and *Pennisetum ciliare*) and soil samples were collected from 46
156 sites along the ~14-km transect on the leeward side of Kohala Mountain, Hawai‘i in July–August
157 of 2018 and/or 2019 and 2021. Aboveground grass matter was cut, collected, weighed, and oven-
158 dried immediately after removal from the field. All collected grasses were weighed after drying to
159 obtain standardized aboveground biomass data. Each soil sample was collected as a continuous
160 10-cm core, manually homogenized and picked through to remove root matter and rocks, sealed
161 in three layers of plastic bags, and frozen. Soil subsamples were sieved to 2 mm, weighed, oven-
162 dried at 65˚C until dry, weighed again to gravimetrically determine percent soil moisture, and
163 ground with mortar and pestle.

164 Sampling soil to 10 cm allows for consistent sampling depth in all sites and focuses
165 analyses within a biologically and redox active region within the soil profile: 10-cm soil depth
166 spans much of the grass rooting zone and extends deep enough to capture oxic-anoxic interfaces,
167 hotspots of redox activity and organic C oxidation (Hall et al., 2015; Jones et al., 2018).

168

169 *2.3 Field Study: CO_2 Measurements*

170 To measure gas efflux from soil collected along the gradient, we constructed air-tight gas chambers
171 using 236.5ml mason jars and compression fittings (Figures S3A, B). In each lid, a compression
172 fitting sealed a butyl plug into a hole drilled to accommodate a syringe needle. Syringes with Luer-
173 lock stopcocks and 22-gauge, 25.4-mm needles (BD, Franklin Lakes, NJ USA) were used to
174 sample gas—the needle was inserted into the sealed gas chamber through the butyl plug, the
175 stopcock was opened, 12 ml of gas was extracted, the stopcock was closed, the needle was
176 withdrawn from the chamber, and the gas sample was transferred to an evacuated 12-ml gas vial
177 (Lampeter, UK) and subsequently analyzed for CO_2 concentration on a Shimadzu 2014 Gas

Chromatograph (GC) in the Environmental Measurements (EM-1) Facility at Stanford University. Gas chambers were tested to confirm they were air-tight before being used to measure soil gas efflux.

In July–August 2021, 10-cm soil cores were collected from 13 sites along the gradient. Soil cores were double bagged in the field and manually homogenized to remove root matter and rocks. Within hours of field collection, equal volumes of soils were divided among gas-chamber mason jars, four jars per site. The soil jars rested undisturbed and uncovered for 24 h before gas sampling commenced. Gas was collected from each chamber at 0, 5, 15, and 30 min. At 0 min, the lid was sealed onto the jar and gas sampled. The gas chambers remained sealed until the final gas sample was taken at 30 min. Ambient temperature was monitored for the duration of gas sampling using a hand-held digital thermometer (Garmin, Olathe, KS USA); temperature data were used to calculate CO_2 flux.

2.4 Field Study: Enzyme Activities

Following methods adapted from Saiya-Cork et al. (2002), we assayed the activities of ligninolytic enzymes peroxidase, MnP, and phenol oxidase in soil samples collected in Summer 2021 (Saiya-Cork et al., 2002). We used 3,3′-5,5′-Tetramethylbenzidine (TMB + 0.3% hydrogen peroxide [H_2O_2]; Kementec, Amherst, NH USA), TMB + 0.3% H_2O_2 + 0.625M manganese sulfate ($MnSO_4$), and 2,2′-azino-bis(3ethylbenzothiazoline-6-sulphonic acid) (ABTS; Sigma Aldrich, St. Louis, MO USA) as substrates to evaluate peroxidase, MnP, and phenol oxidase activities (Floch et al., 2007; Johnsen and Jacobsen, 2008; Kinnunen et al., 2017). For these measurements, 0.45 g field-moist soils were mixed with 45 ml of 50 mM sodium acetate buffer (CH_3 COONa, pH 4.8). Mixtures were vortexed for 30 s, shaken for 3 minutes, and centrifuged at 10,000xg for 1 minute.

Supernatants and enzyme-specific substrates were added to clear, flat-bottomed 96-well microplates (Corning, Corning, NY USA) and incubated at 25ºC for substrate-specific periods determined to maximize potential enzyme activities. Peroxidase and MnP plates incubated for 25 minutes and were stopped and stabilized with 0.2M sulfuric acid (H_2SO_4); phenol oxidase plates incubated for 15 minutes and were stopped and stabilized with 1% sodium dodecyl sulfate (SDS). Absorbances were assessed using a Tecan Infinite M200 Microplate Reader (Männedorf, Switzerland) with emission wavelengths set at 450 nm (for TMB + H_2O_2 and TMB + 0.3% H_2O_2 + $MnSO_4$) or 405 nm (for ABTS). Final enzyme activity values were calculated as described in DeForest (2009) and expressed in units of μmole substrate per hour per g dry soil (μmol $h^{-1}g^{-1}$) (DeForest, 2009; Giambelluca et al., 2013). Reported enzyme activities were measured in 16 reaction wells and averaged for each field site.

2.5 Field Study: Manganese Chemistry

Oven-dried grass samples were shipped to Stanford University, finely ground using a Wiley mill, and analyzed as powders for total Mn (and other metal) content using X-ray fluorescence (XRF) spectrometry (Spectro Xepos HE XRF Spectrometer). Oven-dried, sieved, and finely ground soil samples were also analyzed as powders for Mn and other metal concentrations using XRF spectrometry.

Reduced and organically bound soil Mn was determined using sodium pyrophosphate ($Na_4P_2O_7•10H_2O$) extractions (Carter and Gregorich, 2008; Keiluweit et al., 2015; Qian et al., 2019). In this method, when soil is mixed with Na-pyrophosphate, pyrophosphate chelates organically bound Mn, producing an extractable Mn species (Mn-pyrophosphate) that represents the reduced and organically bound pool of Mn. Accordingly, 0.6 g soil from each site (sampled in

2019 and 2021) was mixed with 30 ml sodium pyrophosphate solution (50mM $Na_4P_2O_7 \bullet 10H_2O$, pH 7.6) and shaken for 16 h at 25°C. The soil slurries were then centrifuged for 10 min @ 20,000xg and filtered to 0.22 μm. DI water was also used as an extractant in parallel to represent the most reduced, non-organically bound Mn pool (Chantigny et al., 2014; Guigue et al., 2014). 6 g of soil was shaken with 24 ml DI water for 45 minutes. Slurries were then centrifuged at 20,000xg for 10 minutes and filtered to 0.22 μm. Mn (and other metal) contents in the Na-pyrophosphate and DI-water extracts were measured using inductively coupled plasma optical emission spectroscopy (ICP-OES) on an Inductively Coupled Plasma Spectrometer ICAP 6300 Duo View. Mn contents in DI-water extracts were subtracted from Na-pyrophosphate extracts to yield the concentrations of organically bound Mn. Reported values (Figure 2C) are differences between Na-pyrophosphate and DI water extract values (Figure 2D) measured in triplicate.

Mn oxidation states in soils were determined using Mn X-ray Near Edge Structure (XANES) Spectroscopy (Lytle et al., 1984). Soils remained frozen until they were loaded and sealed into sample holders using X-ray-transparent Kapton tape; loaded sample holders were kept in the dark at 4°C for 24 h, then flash frozen in liquid nitrogen and run on the XANES instrument.

XRF and ICP-OES measurements were performed in the EM-1 Facility at Stanford University. Mn XANES spectra were measured at the Stanford Synchrotron Radiation Lightsource at SLAC National Accelerator Laboratory (SLAC SSRL) on beamline 9-3 (Lytle et al., 1984).

2.6 Field Study: Carbon and Nitrogen Chemistry

Dried, ground soils were analyzed for C and N content using a Carlo Erba NA 1500 Elemental Analyzer (EA). Frozen, field-moist soils were shaken with DI water (6g:24ml) for 45 minutes to extract dissolved OM. Slurries were centrifuged at 20,000xg for 10 min, and supernatants were

247 filtered to 0.45 μm. Dissolved organic C (DOC) content in extracts was measured on a Shimadzu
248 TOC-L Total Organic Carbon Analyzer; LMWOA (acetate, formate, lactate, and oxalate)
249 concentrations were measured using ion chromatography (IC) on a Dionex DX-500 Ion
250 Chromatograph. EA, TOC, and IC measurements were performed in the EM-1 Facility at Stanford
251 University.
252
253 *2.7 Wet-up Experiment: Soil Sample Collection*
254 Soil samples were collected from a site on the Kohala Mountain rainfall gradient that experiences
255 ~2163 mm MAP. Each soil sample was collected as a continuous 10-cm core from the A horizon,
256 sealed in two layers of plastic bags, manually homogenized to remove root matter and rocks, and
257 frozen at -20°C. Soils remained frozen until 48 h before the experiment's start, at which time they
258 thawed at 20°C while still sealed in plastic bags. 24 h before the experiment's start, we manually
259 homogenized soils again and divided equal masses among the experimental mason jars. The soils
260 were left to settle for 24 h in the open jars until the experiment began.
261 To measure percent soil moisture gravimetrically and to characterize air-dry-to-oven-dry
262 mass conversions, soil subsamples were sieved to 2 mm, weighed, oven-dried at 65˚C until dry,
263 and weighed again. We determined background Mn and DOC contents in, respectively, dried and
264 ground subsamples or thawed subsamples and used the air-dry-to-oven-dry mass conversions to
265 report Mn concentrations and DOC contents for all samples on a dry-weight basis. Field-condition
266 soil subsamples were found to contain 44% moisture ± 7.34% (SD), averaged from triplicate
267 measurements.
268
269 *2.8 Wet-up Experiment*

The experiment was designed to investigate the effect of biologically relevant levels of Mn treatment on SOC stability. In preparation for the experiment, 24 half-pint glass mason jars were acid-washed and sterilized. Thawed soil samples were gently homogenized and randomly assigned to one of three conditions: Control, Moderate Mn, or High Mn. Eight jars belonged to each condition: one jar for soil sampling at each timepoint for 5 timepoints and three jars for gas sampling at each timepoint, totaling 24 jars. Over the course of the experiment, the jars' gas or soil were sampled at 0 h (time of wet up), 0.5 h, 24 h, 72 h, and 120 h.

90 g of thawed, field-moist soil was added to each jar and left to rest at 20°C for 24 h. At Time 0 h, jars received equal volumes of deionized (DI) water (Control), 0.08M manganese chloride ($MnCl_2$) (Moderate Mn), or 0.24M $MnCl_2$ (High Mn) to increase soil moisture from 44% (field-condition moisture) to 65%; 65% allows adequate moisture and air within soil pores to support reduction and oxidation—redox cycling—within the experiment's 120h timeframe (Wen et al., 2019). To avoid damaging the soil's micro-structural integrity and microbial community, we did not dry the soil to 0% before wetting it to 65% moisture content. Instead, we assumed background 44% soil moisture from our measurements in field-condition soils. $MnCl_2$ dilutions were prepared with DI water. Soil Mn concentrations along the Kohala rainfall gradient ranges from ~400–3500 μg Mn g^{-1} dried soil (ppm). Field-condition experimental soils from the site we used contain 1100 ppm Mn. The Moderate Mn group received 0.08M $MnCl_2$ to increase total soil Mn to approximately 2000 ppm, and the High Mn group received 0.24M $MnCl_2$ to raise soil Mn to approximately 4000 ppm.

At Time 0, the jars were wetted with the appropriate treatment; Time 0 soil jars were weighed and then sampled; gas jars were capped for immediate gas collection at 0, 5, 10, and 15 min. We collected gas and soil again at 0.5, 24, 72, and 120 h to monitor changes in CO_2 efflux,

293 DOC and extractable Mn concentrations, and soil moisture. After each soil collection, all soil
294 samples were immediately frozen at -20°C until they could be analyzed.
295
296 *2.9 Wet-up Experiment: CO_2 Sampling*
297 The same air-tight gas chambers used in the field experiment were used in the wet-up experiment
298 (Figures S3C–D). Butyl plugs and seals were replaced, and the gas chambers were retested to
299 confirm they were air-tight before being used to measure soil gas efflux. Gas was collected from
300 each chamber at 0, 5, 10, and 15 minutes—the minute 0 collection occurred at the designated
301 experimental timepoint: 0, 0.5, 24, 72, or 120 h. At minute 0, the lid was sealed onto the jar and
302 gas sampled. The gas chambers remained sealed until the final gas sample was taken at 15 min,
303 after which time the jars remained open until the next experimental sampling timepoint. Gas
304 samples were analyzed for CO_2 concentrations on the GC in the EM-1 Facility at Stanford
305 University.
306
307 *2.10 Wet-up Experiment: Laboratory Analyses*
308 Background Mn content in soils were determined in oven-dried, sieved, and ground samples using
309 XRF. Water-extractable soil Mn, Na-pyrophosphate-extractable soil Mn, and DOC were processed
310 and measured in triplicate in the same manner as described for field samples. Unlike with the field
311 samples, we did not subtract experiment's water-extractable soil Mn values from the Na-
312 pyrophosphate-extractable soil Mn values; the Na-pyrophosphate-extractable soil Mn is assumed
313 to include reduced and organically bound Mn.
314
315 *2.11 Wet-up Experiment: Micro-X-ray Fluorescence Imaging*

316 Mn distribution and oxidation states in soils were determined using elemental maps and Mn
317 μXANES spectra. Synchrotron micro-X-ray absorption spectroscopy (μXAS) and μXRF imaging
318 were performed on beamline 2–3 at the Stanford Synchrotron Radiation Lightsource (SSRL),
319 SLAC National Accelerator Laboratory. This beamline uses a water-cooled, double-crystal
320 Si(111) monochromator; the energy was calibrated using the first derivative of a Mn metal foil to
321 6537.7 eV (Manceau et al., 2012). Soil subsamples for each condition at Time 0 and 72 h were
322 impregnated with epoxy (Epoxy Technology, Billerica, MA), cured, mounted on quartz slides (Ted
323 Pella, Redding, CA), thin-sectioned, and polished at SLAC SSRL.

324 Each soil thin section was initially imaged using coarse resolution to map total Mn
325 abundance. We used these data to choose regions for Mn multi-energy mapping and XANES
326 spectroscopy to map Mn oxidation states across soil surfaces. Fine-resolution images were
327 generated using a 2x2-μm beam focus on small areas of interest. We used principal component
328 analyses (PCA) and simplex volume maximization (SiVM) in SMAK (v2.00) to choose the most
329 appropriate locations for XANES spectroscopy (Webb, 2011; Alfeld et al., 2017; Kravchenko et
330 al., 2022). XANES spectra were normalized and verified in SixPack (v1.5.6) using previously
331 published standards (Hansel et al., 2012; Johnson et al., 2016).

332 To compare relative densities of Mn oxidation states across soil surfaces, we used SMAK
333 to perform particle statistics. Particles were distinguished from backgrounds using InvBinary or
334 Otsu thresholding algorithms, and the minimum-sized particle was defined as two pixels. Regions
335 of Interest (ROI) were assigned by the Particle Statistics function in SMAK following PCA and
336 XANES analyses.

337

338 *2.12 Data and Statistical Analyses*

Means and standard errors of means were calculated for all soil analyses. We applied the Shapiro-Wilk test to assess normality in all datasets. When the data satisfied normality assumptions, we applied the parametric One-way Analysis of Variance (ANOVA) and Tukey's Honest Significant Difference (HSD) post-hoc test to compare the dataset means among Control, Moderate Mn, and High Mn conditions. When the data did not meet normality assumptions, we applied the nonparametric Kruskal-Wallis test and the Dunn-Bonferroni post-hoc test. Significance was determined as p-values ≤ 0.05. Calculations, graphing, and statistics were performed in Microsoft Excel (v16.67) and R (v4.2.2). Synchrotron data were collected using SMAK (v2.00) (Webb, 2011); spectra normalizations and statistics (Principal Component Analyses [PCA] and Linear Combination Fitting [LCF]) were performed using Sixpack (v1.5.6) (Webb et al., 2005) and Athena (v0.9.26) (Ravel and Newville, 2005); fits were verified using previously published standards (Hansel et al., 2012; Johnson et al., 2016; Wen et al., 2022). Kohala gradient mean annual precipitations (MAP) were reported from Giambelluca et al. 2013.

3. Results

3.1 Field Study: Manganese Patterns

To understand how rainfall influences Mn redox cycling, we measured Mn concentrations in three different pools along the gradient that reflect distinct Mn reactivities—soil, grass litter, and bound to OM. Total soil Mn concentrations (Figure 2A) generally decreased as MAP increased. Grass Mn concentrations (Figure 2B) remained low until around 1800 mm MAP, where concentrations rose and then peaked at 1900 mm MAP before diminishing. Organically bound Mn (extractable Mn) (Figure 2C) and water-extractable Mn (Figure 2D) increased in concentration from about 800–1800 mm MAP and then gradually decreased from 1800–2000 mm MAP. Organically bound

362 Mn subtly rose again at the wettest site. Notably, each Mn pool—total soil Mn, plant Mn, and Mn
363 most likely to be oxidized to and stabilized as reactive Mn^{3+}—predominates in distinct rainfall
364 regions along the gradient.

365 XANES analyses of frozen soils revealed trends in Mn oxidation states along the gradient
366 (Figure 2E). Mn^{2+} generally increases in abundance in wetter soils, composing 6% of total soil Mn
367 in the driest site and nearly 60% in the wettest site. Mn^{3+} is relatively abundant in the driest third
368 and wettest third of MAP regions, showing the lowest percentages in the middle of the gradient
369 (from ~900–2000 mm MAP). Mn^{4+} predominates Mn composition in most sites, overshadowing
370 Mn^{2+} and Mn^{3+} percentages from about 800–2000 mm MAP (except at the site receiving 1100 mm
371 MAP); its abundance precipitously declines, however, becoming absent in all but one site receiving
372 more than 2500 mm MAP.

373

374 *3.2 Field Study: Trends in Low-molecular-weight Organic Acids*

375 LMWOA can stabilize Mn^{3+} long enough for the oxidant to diffuse into SOM and oxidize
376 otherwise protected C. We measured LMWOA concentration in soils to identify where along the
377 gradient LMWOA are abundant and to see if patterns in LMWOA abundance overlap with Mn^{3+}
378 cycling along the gradient (Figure 2C, Figure 3). We found that acetate concentrations are greatest
379 below 900 mm MAP, formate concentrations are greatest from 300–1800 mm MAP, lactate
380 concentrations are greatest below 1800 and above 2800 mm MAP, and oxalate concentrations are
381 greatest from 822–1500 mm MAP and around 2900 mm MAP (Figure 3A–D). Formate, lactate,
382 and oxalate showed the most similar patterns, appearing in lowest abundance in the wettest regions
383 of the gradient until around 3000 mm MAP.

384

3.3 Field Study: Trends in Enzyme Activities

MnP is the enzyme responsible for generating most biologically derived Mn^{3+}. We measured its activity along the gradient to investigate how it changes with rainfall and whether its activity pattern overlaps with that of Mn^{3+} cycling (Figure 2C) and metrics of soil C instability (Figures 4B, C). Enzyme activity data are shown in Figure 3E. We also measured peroxidase and phenol oxidase activities to provide context for MnP observations. Phenol oxidase activity remained low for the entire gradient. Peroxidase and MnP activities showed a similar trend: activities were consistently high above 1700 mm MAP, peaking at 1900 mm MAP.

MnP constitutes 99% of ligninolytic-enzyme expression in some systems. In comparison, over the entire gradient, we observed MnP composes an average of 28.5% of total lignin-decay enzyme activity (median is 28.4%), with maxima of 55.9% at 343 mm MAP and 52.5% at 3238 mm MAP (Figure S1D). From 1000–2400 mm MAP, where we found organically bound Mn^{3+} to be greatest, MnP makes up an average of 26.2% of total ligninolytic enzyme activity (median is 27.2%), maxing out at 46.1% at 1808 mm MAP. In this grassland, MnP appears to be a less dominant decay enzyme than it is in temperate and tropical forests (Entwistle et al., 2018; Fujii et al., 2020).

3.4 Field Study: Organic Matter and CO_2 Flux along the Gradient

We found that SOM increases with rainfall along the gradient, indicated by increasing % C and % N with MAP (Figure 4A). These data agree with previous studies on the gradient (von Sperber et al., 2017; Vitousek et al., 2019). Water-extractable DOC showed a bimodal trend: elevated DOC was found from 500–2000 mm MAP (maximum at 1200 mm MAP) and above 2200 mm MAP (Figure 4B). DOC data measured in sites wetter than 1100 mm MAP showed great variability,

illustrated by large standard error of the mean (SEM) values. The greatest DOC concentration was observed in soils collected from the site receiving 1159 mm MAP, followed closely by the sites receiving 2200 and 2700 mm MAP.

Soil CO_2 flux was measured in sites receiving from 459–3123 mm MAP (Figure 4C). Each of these sites was measured four times (n = 4). Along most of the gradient, CO_2 efflux varies between 2.5 and 3.8 mg CO_2 m^{-2} h^{-1}, dipping to the lowest values at sites receiving 1340 and 2238–2686 mm MAP; at the wettest site, CO_2 efflux abruptly jumps to nearly 6 mg CO_2 m^{-2} h^{-1}. The greatest CO_2 flux is from the wettest site, and the next highest efflux values are from the sites receiving 1527 and 2035 mm MAP. CO_2 efflux along the gradient did not follow the linear patterns of %C and %N, nor the bimodal trend of DOC.

3.5 Wet-up Experiment: Soil Moisture

At time 0, following wet-up, the Control, Moderate Mn, and High Mn conditions contained ~65% soil moisture, which endured through 0.5 h (Figure 5a). Soil moisture then steadily decreased, approximating 64% at 24 h, 35% at 72 h, and 16% at 120 h. Within each timepoint, the conditions' soil moistures did not significantly differ.

Qian et al. (2019) found 65% soil moisture to facilitate redox cycling. At the time of sampling, the soil moisture on the Kohala gradient varied from 7% at the dry end to 68% at the wet end. The experimental soil contained 44% soil moisture prior to wet-up (Table S1), 65% at wet-up (Time 0 h), and 16% by the experiment's end at 120 h. The experimental soil experienced environmentally relevant soil moistures for the gradient; the C and Mn dynamics observed over the experiment may suggest how this soil's nutrient cycles could respond to a changing climate,

predicted to cause drier conditions but more frequent and intense rainfall in some areas (IPCC, 2022).

3.6 Wet-up Experiment: Carbon Dynamics

CO_2 flux was measured from the soils at each timepoint by sealing the jars and drawing gas over 15 min. The greatest gas flux across all timepoints was measured at 0.5 h in the Control group (Figure 5B). At this time and at 72 h, the Control group experienced significantly higher CO_2 flux than the Moderate Mn and High Mn groups ($p \leq 0.05$). No statistically significant differences were found at any other timepoint.

Dissolved organic C (DOC) was measured in DI water soil extracts (Figure 5C). A clear pattern emerged and endured through the entirety of the experiment: the Control group extracts contained significantly more DOC than did the Moderate Mn and High Mn groups ($p \leq 0.05$). Furthermore, at every timepoint, DOC was about two-times as concentrated in Control extracts as it was in Moderate Mn and High Mn extracts, which never significantly differed. The data clearly and strongly demonstrate that DOC concentrations negatively correlate with added Mn.

3.7 Wet-up Experiment: Manganese

Table 1 displays the concentrations of Mn measured in deionized (DI) water and sodium-pyrophosphate (NaPP) extracts. The DI water extracts capture the most reduced and energetically stable pool of soil Mn, predominately Mn^{2+}. When shaken with NaPP, organically bound Mn exchanges with sodium ions, forming stable Mn-pyrophosphate complexes. Under natural soil conditions, Mn^{3+} is thermodynamically unstable and must be chelated (typically by LMWOA) to persist. If not chelated, it will rapidly oxidize to Mn^{4+} or reduce to Mn^{2+}, depending on the soil's

453 pH and redox environment. Accordingly, NaPP extractions approximate the reduced and
454 organically bound fractions of Mn, which include Mn^{2+} and Mn^{3+}.

455 DI water and NaPP extracts of field-condition soil contain, respectively, 0.658 μg Mn g^{-1}
456 dried soil (SEM = 0.029) and 201 μg Mn g^{-1} dried soil (SEM = 12.2) (Table S1). All field-condition
457 soils collected along the gradient show this trend in which NaPP extracts contain far greater Mn
458 concentrations than DI water extracts do (~1000:1). Following wet-up, the Control group's soils
459 initially showed a similar pattern; however, the Control group's later sampling periods and the
460 Mn-treated soils diverged. The Control group's ratio of Mn concentrations in NaPP vs. water
461 extracts dropped from 473 at 0 h to 27.2 at 120 h, indicating an increase in soluble Mn relative to
462 organically bound Mn (Table 1). The Moderate Mn group's ratio peaked at 0 h then decreased
463 over 0.5 and 24 h before increasing again. The High Mn group's ratio increased from 0–72 h then
464 slightly decreased at 120 h, settling at 1.52. Intriguingly, over the first 24 h, this group showed
465 greater Mn content in the DI water extracts than in the NaPP, suggesting the added Mn^{2+} (as
466 $MnCl_2$) originally far exceeded the bound Mn fraction; such ratios are not observed in field soils
467 along the gradient.

468 The Control group had the lowest Mn concentrations in both extracts of all conditions. Mn
469 concentrations in DI water extracts did not vary with time; Mn concentrations in the Control NaPP
470 extracts significantly decreased from 72 to 120 h but showed no other differences with time. Mn
471 concentrations in the Moderate Mn DI water extracts approximately doubled from 0 to 0.5 h and
472 then settled halfway between the 0-h and 0.5-h concentrations. The Moderate Mn NaPP extracts
473 showed no differences in Mn concentration over time. The High Mn DI water extracts showed the
474 highest Mn concentrations at 0.5 h and the lowest at 72 and 120 h. In contrast, the High Mn NaPP
475 extracts had the lowest Mn contents at 0 h and the greatest at 72 h.

476 At all timepoints, Mn contents in the Control and the Moderate Mn conditions' extracts
477 were greater when extracted with NaPP than with DI water. The High Mn conditions saw slightly
478 greater Mn concentrations in the DI water extracts than in the NaPP extracts until 72 h, when the
479 NaPP extracts contained significantly more Mn; this ratio held through 120 h.

480 Particle density analyses were performed on thin sections of soils collected from all three
481 conditions at Time 0 and 72 h (Figure 5D). The particle density analysis reveals the relative
482 compositions of Mn^{2+}, Mn^{3+}, and Mn^{4+} across the soil-sample surfaces. The μ-X-ray Absorption
483 Spectroscopy (μXAS) images on which the particle density analyses were performed are shown
484 in Figure S4. From Time 0 to 72 h, the overall compositions in Mn oxidations states do not
485 significantly change within any experimental condition. The Control condition showed the greatest
486 compositions of Mn^{4+} and Mn^{3+}; the High Mn condition showed the greatest levels of Mn^{2+} and
487 the lowest concentrations of Mn^{3+} and Mn^{4+}; and the Moderate Mn condition presented
488 intermediate levels of all Mn oxidation states relative to the other two conditions. These data reveal
489 that $MnCl_2$ addition enhances Mn^{2+} relative to Mn^{3+} and Mn^{4+} and that these relationships persist
490 over time at the soil surface.

491

492 **4. Discussion**

493 *4.1 Field Study: Manganese and Soil C Stability along the Rainfall Gradient*

494 If Mn is a significant controller of SOC stability, we would expect to see the greatest SOC
495 instability correlate with Mn^{3+} redox activity or with Mn^{4+} abundance—the two oxidizing Mn
496 species. We profiled Mn oxidation states, Mn redox reactivity, soil DOC concentrations, and CO_2
497 efflux along the rainfall gradient to investigate whether Mn correlates with SOC instability.

Each Mn oxidation state can directly or indirectly degrade SOM. Mn^{2+} negatively correlates with SOC storage (Stendahl et al., 2017; Kranabetter, 2019; Hou et al., 2021): it is the bioavailable form of Mn that the fungal enzyme MnP oxidizes to release Mn^{3+}, a diffusible and powerful oxidant that—if chelated by a low-molecular-weight organic molecule (LMWOA) (e.g., citrate)—can directly attack and break down SOM (Hatakka et al., 2003). Mn-oxides are also strong oxidants that occur in soils (Sparks, 2003); these oxides, especially Mn^{4+}-oxides (e.g., birnessite), have been shown to oxidize OM (Chorover and Amistadi, 2001; Xia and Stone, 2019).

Mn^{2+} and Mn^{4+} are more energetically stable than Mn^{3+} is (Bartlett and James, 1993; Stumm and Morgan, 1996; Luther, 2005). Even if chelated, Mn^{3+} is unstable. This instability makes Mn^{3+} a particularly potent oxidant and likely limits its existence to systems where redox conditions fluctuate (Peiffer et al., 2021; Wen et al., 2022). If redox conditions remain oxic or anoxic for too long, Mn^{3+} will oxidize or reduce to more energetically favorable Mn states: Mn^{4+} or Mn^{2+} (Ehrlich, 1987; Luther, 2005, 2010). Accordingly, in addition to profiling Mn oxidation states along the rainfall gradient, we investigated where Mn^{3+} is most likely to cycle by measuring standard reduction potentials, LMWOA concentrations, MnP activity, and organically bound/extractable Mn concentrations. These patterns in combination with those of OM, DOC, and CO_2 efflux reveal the lack of a clear relationship between Mn and SOC.

OM increases with rainfall along the gradient (Figure 4A), and DOC does not show a clear pattern in concentration, except possibly in the wettest site where its concentration plummets to its nadir (Figure 4B). As SOM breaks down, DOC is released then quickly disappears from circulation as it sorbs onto mineral surfaces or degrades into its constituents and CO_2 (Mcdowell and Wood, 1984; Qualls and Haines, 1991; Herbert and Bertsch, 1995). Therefore, DOC concentrations should decrease where it is being oxidized to CO_2 and lost to the atmosphere. Soil CO_2 efflux

showed a similar lack of trend until the wettest site (Figure 4C)—here, CO_2 efflux increased drastically. The low DOC concentration and high CO_2 efflux measured at the wettest site indicates that SOC turnover is greatest on the gradient in this site, as is the pool size of SOM.

Total Mn (Figure 2A) and Mn^{4+} (Figure 2E) decrease with higher rainfall, showing lowest abundance where CO_2 efflux is greatest. Plant-available Mn (Figure 2B) and Mn^{2+} (Figure 2E) follow an opposite trend, generally increasing with rainfall. The bioavailable form of Mn is Mn^{2+} (Marschner, 1988; Alejandro et al., 2020), so plant Mn suggests how the most accessible pool of Mn^{2+} changes along the gradient. Plant Mn concentrations increase with rainfall until the wettest few sites, in which plant Mn drops off. This decrease in concentration is likely due to the heavy rainfall leaching reduced Mn through the soil profile to below the rooting zone, where it is inaccessible to plants. XANES measurements reveal Mn^{2+} composes nearly 60% of total Mn in the wettest site; Mn^{3+} composes the other 40%. However, as noted, total soil Mn is low in this site. The redox conditions are oxidizing in the wettest site (likely due to dense root penetration deep into the A horizon); and redox heterogeneity, the temporal variance in standard electromotive potential, is low (Figure S1C). Hence, despite its presence in the soil, Mn^{2+} may not significantly contribute to SOC instability here. The overall Mn abundance is likely too low and redox heterogeneity too narrow for Mn^{2+} to generate sufficient Mn^{3+} to account for the CO_2 efflux and DOC concentration measured in this site.

Direct and indirect measurements of Mn^{3+} cycling corroborate these inferences. LMWOA concentrations suggest where along the gradient Mn^{3+} can be chaperoned, MnP enzyme activity indicates where it can be generated, redox heterogeneity implies where Mn can cycle, and organically bound/extractable Mn concentrations show where it can exist. XANES measurements specify the pattern in persistent soil Mn^{3+}, the Mn^{3+} that is stabilized in the mineral form and not

as redox responsive as organically bound Mn^{3+}. Together, these data illustrate that Mn^{3+} is most redox active and, therefore, most likely to destabilize SOC between 1000–2400 mm MAP. This range does not overlap with where we observed the lowest DOC concentrations or greatest CO_2 efflux, suggesting Mn^{3+} redox cycling in the top 10 cm of soil does not significantly destabilize SOC on the gradient.

4.2 Wet-up Experiment: Does Mn concentration influence the stability of organic carbon in a grassland soil?

Numerous studies have demonstrated a strong positive correlation between Mn availability and OC decomposition (Berg, 2000; Berg et al., 2007, 2010; Davey et al., 2007; Keiluweit et al., 2015; Trum et al., 2015; Kranabetter, 2019). Mn has even been described as the "single main factor" influencing litter decomposition rates and was found to be the strongest predictor of SOC (Berg et al., 2010; Stendahl et al., 2017). These studies were completed in temperate forests or with litter and soil collected from temperate forests. One study on a temperate grassland found that differences in species' sensitivities to Mn toxicity reshaped the plant community—the grassland was treated with N for a decade, acidifying the soil and increasing Mn bioavailability to toxic levels. Consequently, the once forb- and grass-composed community shifted to one exclusively of grasses (forbs are more sensitive to Mn toxicity) (Tian et al., 2016). A follow-up study observed that greater N additions correlated with greater Mn liberation and increased litter decomposition rates (Hou et al., 2021). Such shifts in litter biomass, quality, and decomposition rates suggest that Mn may shape an ecosystem's C cycle. But how Mn does so remains unclear, especially in grasslands, where the evidence is not as robust as it is in temperate forests.

566 We observed that the Control incubations experienced greater DOC and CO_2 releases than
567 the Moderate Mn and High Mn treatment groups did. The wet-up at Time 0 mimicked a heavy
568 rainfall event; in natural soils, rainfall dissolves the soluble fraction of SOM, which can then be
569 lost as leachate or as CO_2 from microbial decomposition (Mcdowell and Wood, 1984; Vance and
570 David, 1992; David et al., 1995; Neff and Asner, 2001). If Mn potentiates C loss from a grassland
571 soil, DOC and CO_2 release should correlate with Mn concentration (Trum et al., 2011; Berg et al.,
572 2015). We observed the opposite, however (Figures 5B, C). In fact, DOC concentrations in Mn-
573 treated soils remained approximately 50% of concentrations measured in the Control soils.
574 NaPP extractions (Table 1), μXAS imaging, and particle density analyses (Figure 5D)
575 confirm that Mn treatments increased the bioavailable fractions of Mn relative to the Control
576 condition. These data illustrate that Mn^{2+} and Mn^{3+} dominate the soil surface and soluble fraction
577 of total Mn—the pools directly interacting with the released DOC. Both Mn oxidation states can
578 bind with DOC: Mn^{3+} requires an organic chelator to persist as a diffusible oxidant (Hatakka et
579 al., 2003), and Mn^{2+} can form outer-sphere complexes with organic acids (Deczky and Langford,
580 1978; Rainville and Weber, 1982; Chen and Gunn, 1990; Radoykova et al., 2015). Therefore, it is
581 possible that the Mn treatment bound DOC, preventing its oxidation and eventual loss as CO_2. The
582 additional Mn swamped the soil system, slowing rather than potentiating SOC turnover.
583 Background evidence collected from this soil and other sites along the Kohala gradient
584 demonstrate that Mn cycling occurs in the field (Figures 2A–E, Figure 3E, Table S1); Mn^{2+} and
585 Mn^{3+} coexist in the soil, soluble, and extractable pools (Table 1, Figure 5D, Table S1, Figure S4,
586 and Figure S5); the soil moisture and pH environment are appropriate (Figure 5A and Table S1);
587 and MnP is produced (Table S1). However, MnP composes approximately 31% of ligninolytic
588 enzyme activity in this soil. MnP can dominate ligninolytic-enzyme expression in ecosystems

589 (Entwistle et al., 2018), and it is the only enzyme dependent on Mn^{2+} (Paszczyński et al., 1986;
590 Brown et al., 1991; Li et al., 1995; Sigoillot et al., 2012).

591 White-rot fungi are the most efficient lignin-degrading fungi, producing a suite of lignin-
592 degrading enzymes that includes MnP (Hofrichter, 2002; Abbas et al., 2005; Wong, 2009;
593 Dashtban et al., 2010; Hatakka and Hammel, 2011). These fungi are ubiquitous and well-studied
594 in forest soils (Cairney, 2005). Their role in grasslands has received less attention. Evidence
595 suggests they are present and active in grasslands, but they appear to be less abundant than they
596 are in forests (Thorn et al., 1996; Gramss, 1997; Deacon et al., 2006; Lynch and Thorn, 2006;
597 Robinson et al., 2009; Kabuyah et al., 2012). Peay et al. 2017 reported basidiomycete and overall
598 fungal abundance increase with MAP along the gradient; this soil is rich with fungal DNA,
599 especially with that of white-rot fungi. DNA can persist in the environment long after its source
600 organism has expired, making it difficult to infer if DNA abundance reflects current or legacy
601 communities (Pochon et al., 2017). In contrast, enzyme activity reveals current conditions—the
602 organisms must be alive to produce active enzymes.

603 The divergence in patterns between fungal DNA abundance and MnP activity can be
604 interpreted in a few ways. If the DNA reflects current conditions, then the basidiomycetes on the
605 gradient are not producing MnP as expected—the basidiomycetes in the middle of the gradient are
606 producing much more MnP than the fungi are in the wettest sites; MnP is more likely to be active
607 in the mildly acidic soil found in the middle of the gradient than it is in the wettest region's ~pH 4
608 soil (Figure S1A) (Fujii et al., 2013). If the DNA is vestigial, then the MnP activity may reveal
609 where basidiomycetes are currently abundant and active. In either scenario, the ratio of MnP
610 activity to total ligninolytic enzyme activity suggest that MnP (and fungal Mn cycling) is not the
611 primary mechanism for SOC turnover in this grassland soil. The system is adapted to the natural

612 Mn levels found in this soil. Adding bioavailable Mn did not increase SOC turnover; it merely
613 flooded the soil.
614
615 **5. Conclusions**
616 Our field and experimental findings suggest that Mn does not control SOC turnover in this
617 grassland. Our measurements were limited to the top 10 cm of soil, so it is possible investigations
618 deeper in the soil profile could reveal greater Mn influence. It is notable, however, that MnP
619 enzyme activity did not compose more than 55% of total enzyme activity anywhere on the gradient.
620 Peay et al. (2017) found that fungal (specifically basidiomycete) abundance on the gradient
621 correlates with rainfall. Therefore, the pattern in MnP activity we observed does not necessarily
622 result from a decline in fungal population.
623 Our findings also reflect the soil's current conditions and microbial activity. Under
624 changing climate conditions, the microbial community composition could shift and adapt to
625 increased Mn bioavailability. Further study is warranted on the current and potential functioning
626 of Mn redox cycling in this and other grasslands to understand how this ecosystem's C stocks
627 respond or could respond to climate change.
628 Most studies that have demonstrated that Mn abundance potentiates SOC loss were done
629 in temperate forests (Berg, 2000; Berg et al., 2007, 2015; Keiluweit et al., 2015; Stendahl et al.,
630 2017; Jones et al., 2018). Our findings provide evidence that this relationship does not persist
631 across all ecosystems. OM stability is an ecosystem property, reflecting the abiotic and biotic
632 environment (Schmidt et al., 2011; Lehmann and Kleber, 2015). A soil's environmental factors—
633 its total Mn content; mineral composition; structure; texture; water content; and microbial
634 community, activity, and distribution—may override the importance of bioavailable Mn to SOM

635 decomposition (Gramss, 1997; Schmidt et al., 2011; Lehmann and Kleber, 2015; Heckman et al.,
636 2021; Possinger et al., 2022; Santos and Herndon, 2023). The Hawaiian gradient's volcanic soils
637 may limit Mn availability by adsorbing Mn as it does Fe. Future studies should introduce higher-
638 resolution techniques (e.g., X-ray photoelectron spectroscopy and Auger electron spectroscopy)
639 that can parse the C and Mn dynamics at a finer scale. Although Mn does not appear to affect SOC
640 turnover enough to manifest in DOC concentrations or CO_2 efflux, it could influence C dynamics
641 in subtler or slower ways that may yet shape this grassland's nutrient cycle.
642
643 **6. Acknowledgements**
644 This work was supported by United States National Science Foundation Award Number 2027290,
645 in collaboration with Dr. Mengqiang Zhu (University of Wyoming). ELP was also supported by
646 the Department of Energy Science Graduate Student Research Fellowship (DOE SCGSR). The
647 authors thank: Parker Ranch, Ponoholo Ranch, and Kamehameha Schools for access to the
648 research sites; Hawai‘i Preparatory Academy for facilities access; Ulu Mau Puanui for equipment
649 support; Michael Burnett, Kehaulani Marshall, and Healohamele Genovia for field assistance;
650 Doug Turner and Dr. Guangchao Li for laboratory analyses; Drs. Juan Lezama, Kristin Boye, Sam
651 Webb, Leah Kelly, and Matthew Latimer for SLAC SSRL synchrotron data collection and
652 interpretation; and Drs. Scott Fendorf, Oliver Chadwick, Karen Casciotti, and Kabir Peay of
653 Stanford University for their invaluable input on this work.
654
655 **7. References**

656 Abbas, A., Koc, H., Liu, F., Tien, M., 2005. Fungal degradation of wood: initial proteomic
657 analysis of extracellular proteins of Phanerochaete chrysosporium grown on oak
658 substrate. Current Genetics 47, 49–56. doi:10.1007/s00294-004-0550-4

659 Alejandro, S., Höller, S., Meier, B., Peiter, E., 2020. Manganese in Plants: From Acquisition to
660 Subcellular Allocation. Frontiers in Plant Science 11, 300. doi:10.3389/fpls.2020.00300
661 Alfeld, M., Wahabzada, M., Bauckhage, C., Kersting, K., van der Snickt, G., Noble, P., Janssens,
662 K., Wellenreuther, G., Falkenberg, G., 2017. Simplex Volume Maximization (SiVM): A
663 matrix factorization algorithm with non-negative constrains and low computing demands
664 for the interpretation of full spectral X-ray fluorescence imaging data. Microchemical
665 Journal 132, 179–184. doi:10.1016/j.microc.2017.02.001
666 Austin, W.E., Huddleston, J.H., 1999. Viability of Permanently Installed Platinum Redox
667 Electrodes. Soil Science Society of America Journal 63, 1757–1762.
668 doi:10.2136/sssaj1999.6361757x
669 Baldrian, P., 2006. Fungal laccases – occurrence and properties. FEMS Microbiology Reviews
670 30, 215–242. doi:10.1111/j.1574-4976.2005.00010.x
671 Barlag, R., Nyasulu, F., Starr, R., Silverman, J., Arthasery, P., McMills, L., 2014. A Student-
672 Made Silver–Silver Chloride Reference Electrode for the General Chemistry Laboratory:
673 ∼10 min Preparation. Journal of Chemical Education 91, 766–768.
674 doi:10.1021/ed400722e
675 Bartlett, R.J., James, B.R., 1993. Redox chemistry of soils, in: Advances in Agronomy.
676 Academic Press, San Diego, pp. 151–208.
677 Berg, B., 2000. Litter decomposition and organic matter turnover in northern forest soils. Forest
678 Ecology and Management 133, 13–22. doi:10.1016/S0378-1127(99)00294-7
679 Berg, B., Davey, M.P., De Marco, A., Emmett, B., Faituri, M., Hobbie, S.E., Johansson, M.-B.,
680 Liu, C., McClaugherty, C., Norell, L., Rutigliano, F.A., Vesterdal, L., Virzo De Santo,
681 A., 2010. Factors influencing limit values for pine needle litter decomposition: a
682 synthesis for boreal and temperate pine forest systems. Biogeochemistry 100, 57–73.
683 doi:10.1007/s10533-009-9404-y
684 Berg, B., Erhagen, B., Johansson, M.-B., Nilsson, M., Stendahl, J., Trum, F., Vesterdal, L., 2015.
685 Manganese in the litter fall-forest floor continuum of boreal and temperate pine and
686 spruce forest ecosystems – A review. Forest Ecology and Management 358, 248–260.
687 doi:10.1016/j.foreco.2015.09.021
688 Berg, B., McClaugherty, C., 2003. Plant Litter. Springer Berlin Heidelberg, Berlin, Heidelberg.
689 doi:10.1007/978-3-662-05349-2
690 Berg, B., Steffen, K.T., McClaugherty, C., 2007. Litter decomposition rate is dependent on litter
691 Mn concentrations. Biogeochemistry 82, 29–39. doi:10.1007/s10533-006-9050-6
692 Brown, J.A., Alic, M., Gold, M.H., 1991. Manganese peroxidase gene transcription in
693 Phanerochaete chrysosporium: activation by manganese. Journal of Bacteriology 173,
694 4101–4106. doi:10.1128/jb.173.13.4101-4106.1991
695 Cairney, J.W.G., 2005. Basidiomycete mycelia in forest soils: dimensions, dynamics and roles in
696 nutrient distribution. Mycological Research 109, 7–20. doi:10.1017/S0953756204001753
697 Carter, M.R., Gregorich, E.G. (Eds.), 2008. Soil sampling and methods of analysis, 2nd ed. ed.
698 Canadian Society of Soil Science ; CRC Press, [Pinawa, Manitoba] : Boca Raton, FL.
699 Chadwick, O.A., Gavenda, R.T., Kelly, E.F., Ziegler, K., Olson, C.G., Elliott, W.C., Hendricks,
700 D.M., 2003. The impact of climate on the biogeochemical functioning of volcanic soils.
701 Chemical Geology 202, 195–223. doi:10.1016/j.chemgeo.2002.09.001
702 Chantigny, M.H., Harrison-Kirk, T., Curtin, D., Beare, M., 2014. Temperature and duration of
703 extraction affect the biochemical composition of soil water-extractable organic matter.
704 Soil Biology and Biochemistry 75, 161–166. doi:10.1016/j.soilbio.2014.04.011

705 Chen, R., Gunn, A.M., 1990. Investigation of extent of organic complexation of Mn $^{2+}$ in
706 coloured upland waters by dialysis titration. Environmental Technology 11, 163–168.
707 doi:10.1080/09593339009384851
708 Chorover, J., Amistadi, M.K., 2001. Reaction of forest floor organic matter at goethite, birnessite
709 and smectite surfaces. Geochimica et Cosmochimica Acta 65, 95–109.
710 doi:10.1016/S0016-7037(00)00511-1
711 Ciais, P., Sabine, C., 2013. Carbon and Other Biogeochemical Cycles (Working Group I
712 Contribution to the Fifth Assessment Report of the Intergovernmental Panel on Climate
713 Change No. 5), Climate Change 2013 The Physical Science Basis. IPCC.
714 Clement, B.G., Luther, G.W., Tebo, B.M., 2009. Rapid, oxygen-dependent microbial Mn(II)
715 oxidation kinetics at sub-micromolar oxygen concentrations in the Black Sea suboxic
716 zone. Geochimica et Cosmochimica Acta 73, 1878–1889. doi:10.1016/j.gca.2008.12.023
717 Cotrufo, M.F., Wallenstein, M.D., Boot, C.M., Denef, K., Paul, E., 2013. The Microbial
718 Efficiency-Matrix Stabilization (MEMS) framework integrates plant litter decomposition
719 with soil organic matter stabilization: do labile plant inputs form stable soil organic
720 matter? Global Change Biology 19, 988–995. doi:10.1111/gcb.12113
721 Cui, F., Dolphin, D., 1990. The Role of Manganese in Model Systems Related to Lignin
722 Biodegradation. Holzforschung 44, 279–283. doi:10.1515/hfsg.1990.44.4.279
723 Dashtban, M., Schraft, H., Syed, T.A., Qin, W., 2010. Fungal biodegradation and enzymatic
724 modification of lignin 15.
725 Davey, M.P., Berg, B., Emmett, B.A., Rowland, P., 2007. Decomposition of oak leaf litter is
726 related to initial litter Mn concentrations. Canadian Journal of Botany 85, 16–24.
727 doi:10.1139/b06-150
728 David, M.B., Vance, G.F., Krzyszowska, A.J., 1995. Carbon Controls on Spodosol Nitrogen,
729 Sulfur, and Phosphorus Cycling, in: Carbon Forms and Functions in Forest Soils. John
730 Wiley & Sons, Ltd, Madison, WI, USA, pp. 329–354. doi:10.2136/1995.carbonforms
731 Deacon, L.J., Janie Pryce-Miller, E., Frankland, J.C., Bainbridge, B.W., Moore, P.D., Robinson,
732 C.H., 2006. Diversity and function of decomposer fungi from a grassland soil. Soil
733 Biology and Biochemistry 38, 7–20. doi:10.1016/j.soilbio.2005.04.013
734 Deczky, K., Langford, C.H., 1978. Application of water nuclear magnetic resonance relaxation
735 times to study of metal complexes of the soluble soil organic fraction fulvic acid.
736 Canadian Journal of Chemistry 56, 1947–1951. doi:10.1139/v78-316
737 DeForest, J.L., 2009. The influence of time, storage temperature, and substrate age on potential
738 soil enzyme activity in acidic forest soils using MUB-linked substrates and l-DOPA. Soil
739 Biology and Biochemistry 41, 1180–1186. doi:10.1016/j.soilbio.2009.02.029
740 Dick, G.J., Clement, B.G., Webb, S.M., Fodrie, F.J., Bargar, J.R., Tebo, B.M., 2009. Enzymatic
741 microbial Mn(II) oxidation and Mn biooxide production in the Guaymas Basin deep-sea
742 hydrothermal plume. Geochimica et Cosmochimica Acta 73, 6517–6530.
743 doi:10.1016/j.gca.2009.07.039
744 Ehrlich, H.L., 1987. Manganese oxide reduction as a form of anaerobic respiration.
745 Geomicrobiology Journal 5, 423–431. doi:10.1080/01490458709385977
746 Emerson, S., Kalhorn, S., Jacobs, L., Tebo, B.M., Nealson, K.H., Rosson, R.A., 1982.
747 Environmental oxidation rate of manganese(II): bacterial catalysis. Geochimica et
748 Cosmochimica Acta 46, 1073–1079. doi:10.1016/0016-7037(82)90060-6
749 Entwistle, E.M., Romanowicz, K.J., Argiroff, W.A., Freedman, Z.B., Morris, J.J., Zak, D.R.,
750 2018. Anthropogenic N Deposition Alters the Composition of Expressed Class II Fungal

751 Peroxidases. Applied and Environmental Microbiology 84, e02816-17.
752 doi:10.1128/AEM.02816-17
753 Floch, C., Alarcon-Gutiérrez, E., Criquet, S., 2007. ABTS assay of phenol oxidase activity in
754 soil. Journal of Microbiological Methods 71, 319–324. doi:10.1016/j.mimet.2007.09.020
755 Floudas, D., Binder, M., Riley, R., Barry, K., Blanchette, R.A., Henrissat, B., Martínez, A.T.,
756 Otillar, R., Spatafora, J.W., Yadav, J.S., Aerts, A., Benoit, I., Boyd, A., Carlson, A.,
757 Copeland, A., Coutinho, P.M., de Vries, R.P., Ferreira, P., Findley, K., Foster, B.,
758 Gaskell, J., Glotzer, D., Górecki, P., Heitman, J., Hesse, C., Hori, C., Igarashi, K.,
759 Jurgens, J.A., Kallen, N., Kersten, P., Kohler, A., Kües, U., Kumar, T.K.A., Kuo, A.,
760 LaButti, K., Larrondo, L.F., Lindquist, E., Ling, A., Lombard, V., Lucas, S., Lundell, T.,
761 Martin, R., McLaughlin, D.J., Morgenstern, I., Morin, E., Murat, C., Nagy, L.G., Nolan,
762 M., Ohm, R.A., Patyshakuliyeva, A., Rokas, A., Ruiz-Dueñas, F.J., Sabat, G., Salamov,
763 A., Samejima, M., Schmutz, J., Slot, J.C., St. John, F., Stenlid, J., Sun, H., Sun, S., Syed,
764 K., Tsang, A., Wiebenga, A., Young, D., Pisabarro, A., Eastwood, D.C., Martin, F.,
765 Cullen, D., Grigoriev, I.V., Hibbett, D.S., 2012. The Paleozoic Origin of Enzymatic
766 Lignin Decomposition Reconstructed from 31 Fungal Genomes. Science 336, 1715–
767 1719. doi:10.1126/science.1221748
768 Fujii, K., Nakada, Y., Umezawa, K., Yoshida, M., Shibata, M., Hayakawa, C., Inagaki, Y.,
769 Kosaki, T., Hangs, R., 2020. A comparison of lignin-degrading enzyme activities in
770 forest floor layers across a global climatic gradient. Soil Ecology Letters 2, 281–294.
771 doi:10.1007/s42832-020-0042-6
772 Fujii, K., Uemura, M., Hayakawa, C., Funakawa, S., Kosaki, T., 2013. Environmental control of
773 lignin peroxidase, manganese peroxidase, and laccase activities in forest floor layers in
774 humid Asia. Soil Biology and Biochemistry 57, 109–115.
775 doi:10.1016/j.soilbio.2012.07.007
776 Giambelluca, T.W., Chen, Q., Frazier, A.G., Price, J.P., Chen, Y.-L., Chu, P.-S., Eischeid, J.K.,
777 Delparte, D.M., 2013. Online Rainfall Atlas of Hawai'i. Bulletin of the American
778 Meteorological Society 94, 313–316. doi:10.1175/BAMS-D-11-00228.1
779 Giambelluca, T.W., Shuai, X., Barnes, M., Alliss, R., Longman, R., Miura, T., Chen, Q., Frazier,
780 A., Mudd, R., Cuo, L., Businger, A., 2014. Evapotranspiration of Hawai'i: Final report.
781 US Army Corps of Engineers, Honolulu District, and the Commission on Water Resource
782 Management, State of Hawai'i.
783 Gramss, G., 1997. Activity of oxidative enzymes in fungal mycelia from grassland and forest
784 soils. Journal of Basic Microbiology 37, 407–423. doi:10.1002/jobm.3620370606
785 Guigue, J., Mathieu, O., Lévêque, J., Mounier, S., Laffont, R., Maron, P.A., Navarro, N.,
786 Chateau, C., Amiotte-Suchet, P., Lucas, Y., 2014. A comparison of extraction procedures
787 for water-extractable organic matter in soils: Comparison of WEOM extraction
788 procedures. European Journal of Soil Science 65, 520–530. doi:10.1111/ejss.12156
789 Hall, S.J., Silver, W.L., Timokhin, V.I., Hammel, K.E., 2015. Lignin decomposition is sustained
790 under fluctuating redox conditions in humid tropical forest soils. Global Change Biology
791 21, 2818–2828. doi:10.1111/gcb.12908
792 Hansel, C.M., Learman, D.R., 2016. Geomicrobiology of Manganese, in: Ehrlich, H.L.,
793 Newman, D.K., Kappler, A. (Eds.), Ehrlich's Geomicrobiology. CRC Press, Boca Raton,
794 pp. 401–54.
795 Hansel, C.M., Zeiner, C.A., Santelli, C.M., Webb, S.M., 2012. Mn(II) oxidation by an
796 ascomycete fungus is linked to superoxide production during asexual reproduction.

797 Proceedings of the National Academy of Sciences of the United States of America 109,
798 12621–12625. doi:10.1073/pnas.1203885109
799 Hastings, D., Emerson, S., 1986. Oxidation of manganese by spores of a marine bacillus: Kinetic
800 and thermodynamic considerations. Geochimica et Cosmochimica Acta 50, 1819–1824.
801 doi:10.1016/0016-7037(86)90141-9
802 Hatakka, A., Hammel, K.E., 2011. Fungal Biodegradation of Lignocelluloses, in: Hofrichter, M.
803 (Ed.), Industrial Applications. Springer Berlin Heidelberg, Berlin, Heidelberg, pp. 319–
804 340. doi:10.1007/978-3-642-11458-8_15
805 Hatakka, A., Lundell, T., Hofrichter, M., Maijala, P., 2003. Manganese Peroxidase and Its Role
806 in the Degradation of Wood Lignin, in: Applications of Enzymes to Lignocellulosics,
807 ACS Symposium Series. American Chemical Society, pp. 230–243. doi:10.1021/bk-
808 2003-0855.ch014
809 Heckman, K.A., Nave, L.E., Bowman, M., Gallo, A., Hatten, J.A., Matosziuk, L.M., Possinger,
810 A.R., SanClements, M., Strahm, B.D., Weiglein, T.L., Rasmussen, C., Swanston, C.W.,
811 2021. Divergent controls on carbon concentration and persistence between forests and
812 grasslands of the conterminous US. Biogeochemistry 156, 41–56. doi:10.1007/s10533-
813 020-00725-z
814 Herbert, B.E., Bertsch, P.M., 1995. Characterization of Dissolved and Colloidal Organic Matter
815 in Soil Solution: A Review, in: Carbon Forms and Functions in Forest Soils. John Wiley
816 & Sons, Ltd, pp. 63–88. doi:10.2136/1995.carbonforms.c5
817 Hernandez-Soriano, M.C., Degryse, F., Lombi, E., Smolders, E., 2012. Manganese Toxicity in
818 Barley is Controlled by Solution Manganese and Soil Manganese Speciation. Soil
819 Science Society of America Journal 76, 399–407. doi:10.2136/sssaj2011.0193
820 Hofrichter, M., 2002. Review: lignin conversion by manganese peroxidase (MnP). Enzyme and
821 Microbial Technology 30, 454–466. doi:10.1016/S0141-0229(01)00528-2
822 Hou, S.-L., Hättenschwiler, S., Yang, J.-J., Sistla, S., Wei, H.-W., Zhang, Z.-W., Hu, Y.-Y.,
823 Wang, R.-Z., Cui, S.-Y., Lü, X.-T., Han, X.-G., 2021. Increasing rates of long-term
824 nitrogen deposition consistently increased litter decomposition in a semi-arid grassland.
825 New Phytologist 229, 296–307. doi:10.1111/nph.16854
826 IPCC, 2022. Climate Change and Land: IPCC Special Report on Climate Change,
827 Desertification, Land Degradation, Sustainable Land Management, Food Security, and
828 Greenhouse Gas Fluxes in Terrestrial Ecosystems, 1st ed. Cambridge University Press.
829 doi:10.1017/9781009157988
830 Janusz, G., Kucharzyk, K.H., Pawlik, A., Staszczak, M., Paszczynski, A.J., 2013. Fungal laccase,
831 manganese peroxidase and lignin peroxidase: Gene expression and regulation. Enzyme
832 and Microbial Technology 52, 1–12. doi:10.1016/j.enzmictec.2012.10.003
833 Johnsen, A.R., Jacobsen, O.S., 2008. A quick and sensitive method for the quantification of
834 peroxidase activity of organic surface soil from forests. Soil Biology and Biochemistry
835 40, 814–821. doi:10.1016/j.soilbio.2007.10.017
836 Johnson, J.E., Webb, S.M., Ma, C., Fischer, W.W., 2016. Manganese mineralogy and diagenesis
837 in the sedimentary rock record. Geochimica et Cosmochimica Acta 173, 210–231.
838 doi:10.1016/j.gca.2015.10.027
839 Jones, M.E., Nico, P.S., Ying, S., Regier, T., Thieme, J., Keiluweit, M., 2018. Manganese-
840 Driven Carbon Oxidation at Oxic–Anoxic Interfaces. Environmental Science &
841 Technology 52, 12349–12357. doi:10.1021/acs.est.8b03791
842 Jones, R., 1966. Oxidation-reduction potential measurement. ISA JOURNAL 13, 40.

843 Jost, D., Haberer, C.M., Grathwohl, P., Winter, J., Gallert, C., 2015. Oxygen Transfer in a
844 Fluctuating Capillary Fringe: Impact of Microbial Respiratory Activity. Vadose Zone
845 Journal 14, vzj2014.04.0039. doi:10.2136/vzj2014.04.0039
846 Jung, H., S. Chadha, T., Kim, D., Biswas, P., Jun, Y.-S., 2017. Photochemically assisted fast
847 abiotic oxidation of manganese and formation of δ-MnO 2 nanosheets in nitrate solution.
848 Chemical Communications 53, 4445–4448. doi:10.1039/C7CC00754J
849 Kabuyah, R.N.T.M., van Dongen, B.E., Bewsher, A.D., Robinson, C.H., 2012. Decomposition of
850 lignin in wheat straw in a sand-dune grassland. Soil Biology and Biochemistry 45, 128–
851 131. doi:10.1016/j.soilbio.2011.10.014
852 Kagawa, A.K., Vitousek, P.M., 2012. The Ahupua‘a of Puanui: A Resource for Understanding
853 Hawaiian Rain-Fed Agriculture. Pacific Science 66, 161–172. doi:10.2984/66.2.6
854 Keiluweit, M., Gee, K., Denney, A., Fendorf, S., 2018. Anoxic microsites in upland soils
855 dominantly controlled by clay content. Soil Biology and Biochemistry 118, 42–50.
856 doi:10.1016/j.soilbio.2017.12.002
857 Keiluweit, M., Nico, P., Harmon, M.E., Mao, J., Pett-Ridge, J., Kleber, M., 2015. Long-term
858 litter decomposition controlled by manganese redox cycling. Proceedings of the National
859 Academy of Sciences 112, E5253–E5260. doi:10.1073/pnas.1508945112
860 Keiluweit, M., Nico, P.S., Kleber, M., Fendorf, S., 2016. Are oxygen limitations under
861 recognized regulators of organic carbon turnover in upland soils? Biogeochemistry 127,
862 157–171. doi:10.1007/s10533-015-0180-6
863 Kinnunen, A., Maijala, P., Jarvinen, P., Hatakka, A., 2017. Improved Efficiency in Screening for
864 Lignin-Modifying Peroxidases and Laccases of Basidiomycetes. Current Biotechnology
865 6, 105–115. doi:10.2174/2211550105666160330205138
866 Kirk, T.K., Farrell, R.L., 1987. Enzymatic “Combustion”: The Microbial Degradation of Lignin.
867 Annual Review of Microbiology 41, 465–501.
868 doi:10.1146/annurev.mi.41.100187.002341
869 Köchy, M., Hiederer, R., Freibauer, A., 2015. Global distribution of soil organic carbon – Part 1:
870 Masses and frequency distributions of SOC stocks for the tropics, permafrost regions,
871 wetlands, and the world. SOIL 1, 351–365. doi:10.5194/soil-1-351-2015
872 Kranabetter, J.M., 2019. Increasing soil carbon content with declining soil manganese in
873 temperate rainforests: is there a link to fungal Mn? Soil Biology and Biochemistry 128,
874 179–181. doi:10.1016/j.soilbio.2018.11.001
875 Kravchenko, A.N., Richardson, J.A., Lee, J.H., Guber, A.K., 2022. Distribution of Mn Oxidation
876 States in Grassland Soils and Their Relationships with Soil Pores. Environmental Science
877 & Technology 56, 16462–16472. doi:10.1021/acs.est.2c05403
878 Lan, S., Wang, X., Xiang, Q., Yin, H., Tan, W., Qiu, G., Liu, F., Zhang, J., Feng, X., 2017.
879 Mechanisms of Mn(II) catalytic oxidation on ferrihydrite surfaces and the formation of
880 manganese (oxyhydr)oxides. Geochimica et Cosmochimica Acta 211, 79–96.
881 doi:10.1016/j.gca.2017.04.044
882 Learman, D.R., Wankel, S.D., Webb, S.M., Martinez, N., Madden, A.S., Hansel, C.M., 2011.
883 Coupled biotic–abiotic Mn(II) oxidation pathway mediates the formation and structural
884 evolution of biogenic Mn oxides. Geochimica et Cosmochimica Acta 75, 6048–6063.
885 doi:10.1016/j.gca.2011.07.026
886 Lehmann, J., Kleber, M., 2015. The contentious nature of soil organic matter. Nature 528, 60–68.
887 doi:10.1038/nature16069

888 Li, D., Alic, M., Brown, J.A., Gold, M.H., 1995. Regulation of manganese peroxidase gene
889 transcription by hydrogen peroxide, chemical stress, and molecular oxygen. Applied and
890 Environmental Microbiology 61, 341–345. doi:10.1128/aem.61.1.341-345.1995
891 Luther, G.W., 2010. The Role of One- and Two-Electron Transfer Reactions in Forming
892 Thermodynamically Unstable Intermediates as Barriers in Multi-Electron Redox
893 Reactions. Aquatic Geochemistry 16, 395–420. doi:10.1007/s10498-009-9082-3
894 Luther, G.W., 2005. Manganese(II) Oxidation and Mn(IV) Reduction in the Environment—Two
895 One-Electron Transfer Steps Versus a Single Two-Electron Step. Geomicrobiology 22,
896 195–203. doi:10.1080/01490450590946022
897 Lynch, M.D.J., Thorn, R.G., 2006. Diversity of Basidiomycetes in Michigan Agricultural Soils.
898 Applied and Environmental Microbiology 72, 7050–7056. doi:10.1128/AEM.00826-06
899 Lytle, F.W., Greegor, R.B., Sandstrom, D.R., Marques, E.C., Wong, J., Spiro, C.L., Huffman,
900 G.P., Huggins, F.E., 1984. Measurement of soft X-ray absorption spectra with a
901 fluorescent ion chamber detector. Nuclear Instruments and Methods in Physics Research
902 Section A: Accelerators, Spectrometers, Detectors and Associated Equipment 226, 542–
903 548. doi:10.1016/0168-9002(84)90077-9
904 Madden, A.S., Hochella, M.F., 2005. A test of geochemical reactivity as a function of mineral
905 size: Manganese oxidation promoted by hematite nanoparticles. Geochimica et
906 Cosmochimica Acta 69, 389–398. doi:10.1016/j.gca.2004.06.035
907 Manceau, A., Marcus, M.A., Grangeon, S., 2012. Determination of Mn valence states in mixed-
908 valent manganates by XANES spectroscopy. American Mineralogist 97, 816–827.
909 doi:10.2138/am.2012.3903
910 Marschner, H., 1988. Mechanisms of Manganese Acquisition by Roots from Soils, in: Graham,
911 R.D., Hannam, R.J., Uren, N.C. (Eds.), Manganese in Soils and Plants: Proceedings of
912 the International Symposium on 'Manganese in Soils and Plants' Held at the Waite
913 Agricultural Research Institute, The University of Adelaide, Glen Osmond, South
914 Australia, August 22–26, 1988 as an Australian Bicentennial Event. Springer
915 Netherlands, Dordrecht, pp. 191–204. doi:10.1007/978-94-009-2817-6_14
916 Martínez, Á.T., Ruiz-Dueñas, F.J., Martínez, M.J., del Río, J.C., Gutiérrez, A., 2009. Enzymatic
917 delignification of plant cell wall: from nature to mill. Current Opinion in Biotechnology
918 20, 348–357. doi:10.1016/j.copbio.2009.05.002
919 Mcdowell, W.H., Wood, T., 1984. Podzolization: Soil Processes Control Dissolved Organic
920 Carbon Concentrations in Stream Water. Soil Science 137, 23–32.
921 doi:10.1097/00010694-198401000-00004
922 Meentemeyer, V., 1978. Macroclimate and Lignin Control of Litter Decomposition Rates.
923 Ecology 59, 465–472. doi:10.2307/1936576
924 Neff, J.C., Asner, G.P., 2001. Dissolved Organic Carbon in Terrestrial Ecosystems: Synthesis
925 and a Model. Ecosystems 4, 29–48. doi:10.1007/s100210000058
926 Nordstrom, D.K., Wilde, F.D., 2005. Chap. A6, sec. 6.5. Reduction-Oxidation Potential
927 (Electrode Method), in: Field Measurements: U.S. Geological Survey Techniques of
928 Water-Resources Investigations. USGS, p. 22.
929 Paszczyński, A., Huynh, V.B., Crawford, R., 1986. Comparison of ligninase-I and peroxidase-
930 M2 from the white-rot fungus Phanerochaete chrysosporium. Archives of Biochemistry
931 and Biophysics 244, 750–765. doi:10.1016/0003-9861(86)90644-2
932 Paul, E. (Ed.), 2006. Soil Microbiology, Ecology and Biochemistry, 3rd ed. Academic Press.

933 Peay, K.G., von Sperber, C., Cardarelli, E., Toju, H., Francis, C.A., Chadwick, O.A., Vitousek,
934 P.M., 2017. Convergence and contrast in the community structure of Bacteria, Fungi and
935 Archaea along a tropical elevation–climate gradient. FEMS Microbiology Ecology 93,
936 fix045. doi:10.1093/femsec/fix045
937 Peiffer, S., Kappler, A., Haderlein, S.B., Schmidt, C., Byrne, J.M., Kleindienst, S., Vogt, C.,
938 Richnow, H.H., Obst, M., Angenent, L.T., Bryce, C., McCammon, C., Planer-Friedrich,
939 B., 2021. A biogeochemical–hydrological framework for the role of redox-active
940 compounds in aquatic systems. Nature Geoscience 14, 264–272. doi:10.1038/s41561-
941 021-00742-z
942 Pochon, X., Zaiko, A., Fletcher, L.M., Laroche, O., Wood, S.A., 2017. Wanted dead or alive?
943 Using metabarcoding of environmental DNA and RNA to distinguish living assemblages
944 for biosecurity applications. PLOS ONE 12, e0187636.
945 doi:10.1371/journal.pone.0187636
946 Possinger, A.R., Heckman, K.A., Bowman, M.M., Gallo, A.C., Hatten, J.A., Matosziuk, L.M.,
947 Nave, L.E., SanClements, M.D., Swanston, C.W., Weiglein, T.L., Strahm, B.D., 2022.
948 Lignin and fungal abundance modify manganese effects on soil organic carbon
949 persistence at the continental scale. Geoderma 425, 116070.
950 doi:10.1016/j.geoderma.2022.116070
951 Qian, A., Zhang, W., Shi, C., Pan, C., Giammar, D.E., Yuan, S., Zhang, H., Wang, Z., 2019.
952 Geochemical Stability of Dissolved Mn(III) in the Presence of Pyrophosphate as a Model
953 Ligand: Complexation and Disproportionation. Environmental Science & Technology 53,
954 5768–5777. doi:10.1021/acs.est.9b00498
955 Qualls, R.G., Haines, B.L., 1991. Geochemistry of Dissolved Organic Nutrients in Water
956 Percolating through a Forest Ecosystem. Soil Science Society of America Journal 55,
957 1112–1123. doi:10.2136/sssaj1991.03615995005500040036x
958 Radoykova, T.H., Dimitrova, S.V., Aleksieva, K.I., Nenkova, S.K., Valchev, I.V., Mehandjiev,
959 D.R., 2015. Comparative Mn2+ Adsorption on Waste Lignocellulosic Materials. Journal
960 of Environmental Protection and Ecology 16, 23–32.
961 Rainville, D.P., Weber, J.H., 1982. Complexing capacity of soil fulvic acid for
962 Cu2+,Cd2+,Mn2+,Ni2+,and Zn2+measured by dialysis titration: a model based on soil
963 fulvic acid aggregation. Canadian Journal of Chemistry 60, 1–5. doi:10.1139/v82-001
964 Ravel, B., Newville, M., 2005. ATHENA, ARTEMIS, HEPHAESTUS: data analysis for X-ray
965 absorption spectroscopy using IFEFFIT. Journal of Synchrotron Radiation 12, 537–541.
966 doi:10.1107/S0909049505012719
967 Rezanezhad, F., Couture, R.-M., Kovac, R., O'Connell, D., Van Cappellen, P., 2014. Water table
968 fluctuations and soil biogeochemistry: An experimental approach using an automated soil
969 column system. Journal of Hydrology 509, 245–256. doi:10.1016/j.jhydrol.2013.11.036
970 Riley, R., Salamov, A.A., Brown, D.W., Nagy, L.G., Floudas, D., Held, B.W., Levasseur, A.,
971 Lombard, V., Morin, E., Otillar, R., Lindquist, E.A., Sun, H., LaButti, K.M., Schmutz, J.,
972 Jabbour, D., Luo, H., Baker, S.E., Pisabarro, A.G., Walton, J.D., Blanchette, R.A.,
973 Henrissat, B., Martin, F., Cullen, D., Hibbett, D.S., Grigoriev, I.V., 2014. Extensive
974 sampling of basidiomycete genomes demonstrates inadequacy of the white-rot/brown-rot
975 paradigm for wood decay fungi. Proceedings of the National Academy of Sciences 111,
976 9923–9928. doi:10.1073/pnas.1400592111

977 Robinson, C.H., Szaro, T.M., Izzo, A.D., Anderson, I.C., Parkin, P.I., Bruns, T.D., 2009. Spatial
978 distribution of fungal communities in a coastal grassland soil. Soil Biology and
979 Biochemistry 41, 414–416. doi:10.1016/j.soilbio.2008.10.021
980 Saiya-Cork, K.R., Sinsabaugh, R.L., Zak, D.R., 2002. The effects of long term nitrogen
981 deposition on extracellular enzyme activity in an Acer saccharum forest soil. Soil
982 Biology and Biochemistry 34, 1309–1315. doi:10.1016/S0038-0717(02)00074-3
983 Santelli, C.M., Webb, S.M., Dohnalkova, A.C., Hansel, C.M., 2011. Diversity of Mn oxides
984 produced by Mn(II)-oxidizing fungi. Geochimica et Cosmochimica Acta 75, 2762–2776.
985 doi:10.1016/j.gca.2011.02.022
986 Santos, F., Herndon, E., 2023. Plant-Soil Relationships Influence Observed Trends Between
987 Manganese and Carbon Across Biomes. Global Biogeochemical Cycles 37,
988 e2022GB007412. doi:10.1029/2022GB007412
989 Schmidt, M.W.I., Torn, M.S., Abiven, S., Dittmar, T., Guggenberger, G., Janssens, I.A., Kleber,
990 M., Kögel-Knabner, I., Lehmann, J., Manning, D.A.C., Nannipieri, P., Rasse, D.P.,
991 Weiner, S., Trumbore, S.E., 2011. Persistence of soil organic matter as an ecosystem
992 property. Nature 478, 49–56. doi:10.1038/nature10386
993 Schulze, D.G., Sutton, S.R., Bajt, S., 1995. Determining Manganese Oxidation State in Soils
994 Using X-ray Absorption Near-Edge Structure (XANES) Spectroscopy. Soil Science
995 Society of America Journal 59, 1540–1548.
996 doi:10.2136/sssaj1995.03615995005900060005x
997 Sherrod, D.R., Sinton, J.M., Watkins, S.E., Brunt, K.M., 2007. Geologic Map of the State of
998 Hawai‘i 85.
999 Sigoillot, J.-C., Berrin, J.-G., Bey, M., Lesage-Meessen, L., Levasseur, A., Lomascolo, A.,
1000 Record, E., Uzan-Boukhris, E., 2012. Fungal Strategies for Lignin Degradation, in:
1001 Advances in Botanical Research. Elsevier, pp. 263–308. doi:10.1016/B978-0-12-416023-
1002 1.00008-2
1003 Sparks, D.L., 2003. Environmental Soil Chemistry, 2nd ed. Academic Press, London.
1004 Stendahl, J., Berg, B., Lindahl, B.D., 2017. Manganese availability is negatively associated with
1005 carbon storage in northern coniferous forest humus layers. Scientific Reports 7, 15487.
1006 doi:10.1038/s41598-017-15801-y
1007 Stumm, W., Morgan, J.J., 1996. Aquatic chemistry: chemical equilibria and rates in natural
1008 waters, 3rd ed. ed, Environmental science and technology. Wiley, New York.
1009 Tebo, B.M., Bargar, J.R., Clement, B.G., Dick, G.J., Murray, K.J., Parker, D., Verity, R., Webb,
1010 S.M., 2004. Biogenic manganese oxides: Properties and mechanisms of formation.
1011 Annual Review of Earth and Planetary Sciences 32, 287–328.
1012 doi:10.1146/annurev.earth.32.101802.120213
1013 Tebo, B.M., Emerson, S., 1985. Effect of Oxygen Tension, Mn(II) Concentration, and
1014 Temperature on the Microbially Catalyzed Mn(II) Oxidation Rate in a Marine Fjordt.
1015 APPL. ENVIRON. MICROBIOL. 50, 6.
1016 Tebo, B.M., Nealson, K.H., Emerson, S., Jacobs, L., 1984. Microbial mediation of Mn(II) and
1017 Co(II) precipitation at the O_2 /H_2S interfaces in two anoxic fjords1: Mn and Co
1018 microbial precipitation. Limnology and Oceanography 29, 1247–1258.
1019 doi:10.4319/lo.1984.29.6.1247
1020 Thermo Fisher, 2007. Instruction Sheet Thermo Scientific ORP Standard, 5 x 60 mL Bottles,
1021 Cat. No. 967961 Thermo Scientific ORP Standard, 475 mL Bottle, Cat. No. 967901.

1022 Thomas, G.W., 1996. Soil pH and Soil Acidity, in: Methods of Soil Analysis. John Wiley &
1023 Sons, Ltd, pp. 475–490. doi:10.2136/sssabookser5.3.c16
1024 Thorn, R.G., Reddy, C.A., Harris, D., Paul, E.A., 1996. Isolation of saprophytic basidiomycetes
1025 from soil. Applied and Environmental Microbiology 62, 4288–4292.
1026 doi:10.1128/aem.62.11.4288-4292.1996
1027 Tian, Q., Liu, N., Bai, W., Li, L., Chen, J., Reich, P.B., Yu, Q., Guo, D., Smith, M.D., Knapp,
1028 A.K., Cheng, W., Lu, P., Gao, Y., Yang, A., Wang, T., Li, X., Wang, Z., Ma, Y., Han, X.,
1029 Zhang, W.-H., 2016. A novel soil manganese mechanism drives plant species loss with
1030 increased nitrogen deposition in a temperate steppe. Ecology 97, 65–74. doi:10.1890/15-
1031 0917.1
1032 Trum, F., Titeux, H., Cornelis, J.-T., Delvaux, B., 2011. Effects of manganese addition on carbon
1033 release from forest floor horizons. Canadian Journal of Forest Research 41, 643–648.
1034 doi:10.1139/X10-224
1035 Trum, F., Titeux, H., Ponette, Q., Berg, B., 2015. Influence of manganese on decomposition of
1036 common beech (Fagus sylvatica L.) leaf litter during field incubation. Biogeochemistry
1037 125, 349–358. doi:10.1007/s10533-015-0129-9
1038 Turekian, K.K., Wedepohl, K.H., 1961. Distribution of the Elements in Some Major Units of the
1039 Earth's Crust. GSA Bulletin 72, 175–192. doi:10.1130/0016-
1040 7606(1961)72[175:DOTEIS]2.0.CO;2
1041 van der Lee, G., 1999. Anoxic microsites in Douglas fir litter. Soil Biology and Biochemistry 31,
1042 1295–1301. doi:10.1016/S0038-0717(99)00048-6
1043 Vance, G.F., David, M.B., 1992. Dissolved Organic Carbon and Sulfate Sorption by Spodosol
1044 Mineral Horizons. Soil Science 154, 136.
1045 Villalobos, M., Lanson, B., Manceau, A., Toner, B., Sposito, G., 2006. Structural model for the
1046 biogenic Mn oxide produced by Pseudomonas putida. American Mineralogist 91, 489–
1047 502. doi:10.2138/am.2006.1925
1048 Vitousek, P.M., Chadwick, O.A., 2013. Pedogenic Thresholds and Soil Process Domains in
1049 Basalt-Derived Soils. Ecosystems 16, 1379–1395. doi:10.1007/s10021-013-9690-z
1050 Vitousek, P.M., Paulus, E.L., Chadwick, O.A., 2019. Nitrogen dynamics along a climate gradient
1051 on geologically old substrate, Kaua'i, Hawai'i. Oecologia 189, 211–219.
1052 doi:10.1007/s00442-018-4285-1
1053 von Sperber, C., Chadwick, O.A., Casciotti, K.L., Peay, K.G., Francis, C.A., Kim, A.E.,
1054 Vitousek, P.M., 2017. Controls of nitrogen cycling evaluated along a well- characterized
1055 climate gradient. Ecology 98, 1117–1129. doi:10.1002/ecy.1751
1056 Wanzek, T., Keiluweit, M., Baham, J., Dragila, M.I., Fendorf, S., Fiedler, S., Nico, P.S., Kleber,
1057 M., 2018. Quantifying biogeochemical heterogeneity in soil systems. Geoderma 324, 89–
1058 97. doi:10.1016/j.geoderma.2018.03.003
1059 Webb, S.M., 2011. The MicroAnalysis Toolkit: X- ray Fluorescence Image Processing
1060 Software. AIP Conference Proceedings 1365, 196–199. doi:10.1063/1.3625338
1061 Webb, S.M., Dick, G.J., Bargar, J.R., Tebo, B.M., 2005. Evidence for the presence of Mn(III)
1062 intermediates in the bacterial oxidation of Mn(II). Proceedings of the National Academy
1063 of Sciences 102, 5558–5563. doi:10.1073/pnas.0409119102
1064 Wen, K., Chadwick, O.A., Vitousek, P.M., Paulus, E.L., Landrot, G., Tappero, R.V., Kaszuba,
1065 J.P., Luther, G.W., Wang, Z., Reinhart, B.J., Zhu, M., 2022. Manganese Oxidation States
1066 in Volcanic Soils across Annual Rainfall Gradients. Environmental Science &
1067 Technology acs.est.2c02658. doi:10.1021/acs.est.2c02658

1068 Wen, Y., Zang, H., Ma, Q., Evans, C.D., Chadwick, D.R., Jones, D.L., 2019. Is the 'enzyme
1069 latch' or 'iron gate' the key to protecting soil organic carbon in peatlands? Geoderma
1070 349, 107–113. doi:10.1016/j.geoderma.2019.04.023
1071 Whalen, E.D., Smith, R.G., Grandy, A.S., Frey, S.D., 2018. Manganese limitation as a
1072 mechanism for reduced decomposition in soils under atmospheric nitrogen deposition.
1073 Soil Biology and Biochemistry 127, 252–263. doi:10.1016/j.soilbio.2018.09.025
1074 Wolkersdorfer, C., 2008. Water Management at Abandoned Flooded Underground Mines.
1075 Springer Berlin Heidelberg, Berlin, Heidelberg. doi:10.1007/978-3-540-77331-3
1076 Wong, D.W.S., 2009. Structure and Action Mechanism of Ligninolytic Enzymes. Applied
1077 Biochemistry and Biotechnology 157, 174–209. doi:10.1007/s12010-008-8279-z
1078 Xia, X., Stone, A.T., 2019. Mandelic acid and phenyllactic acid "Reaction Sets" for exploring
1079 the kinetics and mechanism of oxidations by hydrous manganese oxide (HMO).
1080 Environmental Science: Processes & Impacts 21, 1038–1051. doi:10.1039/C9EM00128J
1081 Zhang, T., Liu, L., Tan, W., Suib, S.L., Qiu, G., 2021. Formation and transformation of
1082 manganese(III) intermediates in the photochemical generation of manganese(IV) oxide
1083 minerals. Chemosphere 262, 128082. doi:10.1016/j.chemosphere.2020.128082
1084

1085

8. Tables

Table 1. Manganese (Mn) concentrations in deionized (DI) water and sodium-pyrophosphate (NaPP) extracts from each condition's soils, collected at each experimental timepoint. *Moderate Mn* is abbreviated as *Mod. Mn*. The reported values are averaged from three replicates and are shown with their respective standard error of the mean (SEM).

	Sampling Timepoint (h)									
	0		0.5		24		72		120	
Condition, Extractant	Mean ($\mu g\ g^{-1}$ soil)	SEM ($\mu g\ g^{-1}$ soil)	Mean ($\mu g\ g^{-1}$ soil)	SEM ($\mu g\ g^{-1}$ soil)	Mean ($\mu g\ g^{-1}$ soil)	SEM ($\mu g\ g^{-1}$ soil)	Mean ($\mu g\ g^{-1}$ soil)	SEM ($\mu g\ g^{-1}$ soil)	Mean ($\mu g\ g^{-1}$ soil)	SEM ($\mu g\ g^{-1}$ soil)
Control, Water	0.0300	0.0140	0.139	0.110	0.147	0.117	0.169	0.120	0.341	0.320
Mod. Mn, Water	15.7	4.08	41.0	10.4	26.1	1.56	22.2	2.01	18.9	1.57
High Mn, Water	183	19.6	233	6.47	207	6.99	166	7.23	160	10.6
Control, NaPP	14.1	1.04	11.7	2.14	14.7	0.547	18.1	1.89	9.28	0.550
Mod. Mn, NaPP	78.5	22.2	108	17.9	101	6.60	103	7.87	93.1	5.60
High Mn, NaPP	136	8.63	183	44.8	177	11.6	273	22.7	242	37.4

	Sampling Timepoint (h)				
Extract ratios: NaPP/water	0	0.5	24	72	120
Control	473	83.7	99.7	107	27.2
Mod. Mn	4.99	2.62	3.85	4.66	4.92
High Mn	0.747	0.785	0.851	1.65	1.52

9. Figures

Figure 1. Field sites arrayed along a 14-km transect on the Kohala rainfall gradient, Island of Hawaii. Mean annual precipitation (MAP) varies from <300 to >3200 mm. Google Earth map and inset of the Island of Hawaii display the field sites (white dots).

Figure 2. A) Total soil manganese (Mn) concentrations measured in homogenized 10-cm soil cores along the gradient. B) Total Mn concentrations measured in grasses collected along the gradient. C) Organically bound Mn measured as the difference between Mn measured in sodium-pyrophosphate (NaPP) and deionized (DI) water soil extracts. D) Total Mn concentrations measured in DI water extracts from gradient soils. Filled markers symbolize averaged values (n = 3). Error bars represent SEM. E) Relative abundances of Mn oxidation states in homogenized 10-cm soil cores collected along the gradient were determined using X-ray absorption near-edge structure (XANES) spectroscopy, principal component analysis (PCA), and linear combination fitting (LCF). Corresponding spectra and fits are shown in Figure S2. Percentages of Mn^{2+}, Mn^{3+}, and Mn^{4+} composing total soil Mn are illustrated by blue, green, and purple bars, respectively.

Figure 3. A) Acetate, B) formate, C) lactate, and D) oxalate concentrations in deionized (DI) water extracts from homogenized 10-cm soil cores collected from 46 sites along the rainfall gradient; error bars represent standard error of the mean (SEM). E) Enzyme activities measured in soils along the rainfall gradient; hollow markers symbolize peroxidase, black-filled markers manganese (Mn) peroxidase (MnP), and gray-filled markers phenol oxidase enzyme activities.

Figure 4. A) Soil carbon (C) and nitrogen (N) percentages were measured in 10-cm homogenized soil cores collected in 46 sites along the Kohala rainfall gradient; filled and hollow markers represent averaged values (n = 3) of N and C, respectively. B) Dissolved organic carbon (DOC) was measured in deionized (DI) water soil extracts; filled markers symbolize averaged values (n = 3). C) CO_2 efflux measured from soil cores collected from gradient sites. . Soil CO_2 efflux was measured four times in each site (n = 4). Error bars represent standard error of the mean (SEM).

Figure 5. A) Percent soil moisture did not significantly differ among the experimental conditions at any timepoint (n = 4–7). B) The soil CO_2 efflux was statistically greater for the Control group at times 0.5 and 72 h. C) Dissolved organic C (DOC) in Control soils was statistically greater than in Moderate and High Manganese (Mn) soils at all timepoints. Hollow columns represent Control, gray Moderate Mn, and black High Mn conditions' mean values (n=3) for each timepoint. D) The distribution of Mn oxidation states in each condition's soil did not significantly change from time 0 h to 72 h: Control (C), Moderate Mn (M), and High Mn (H). Corresponding μ-X-ray absorption spectroscopy (μ-XAS) maps are shown in Figure S4. Blue columns represent Mn^{2+} composition, green Mn^{3+}, and purple Mn^{4+}. Solid and dashed error bars indicate standard error of the mean (SEM). Asterisks denote statistical significance at $p \leq 0.05$.

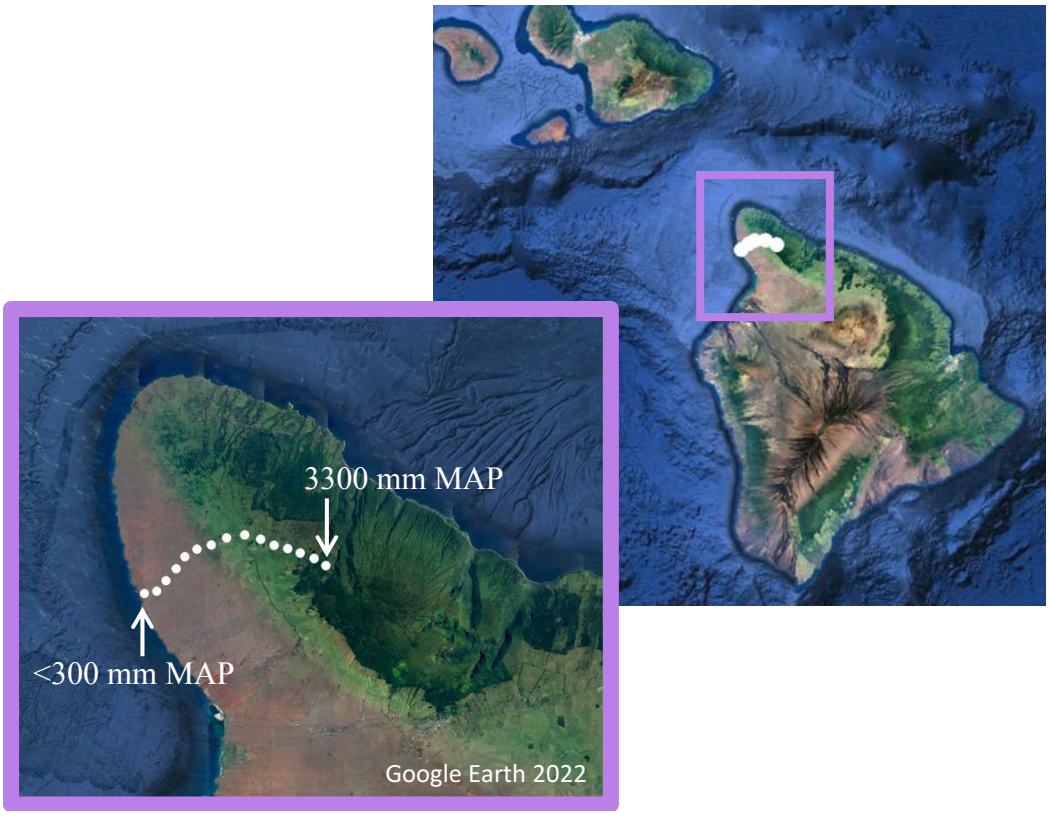

1131

1132

Figure 1.

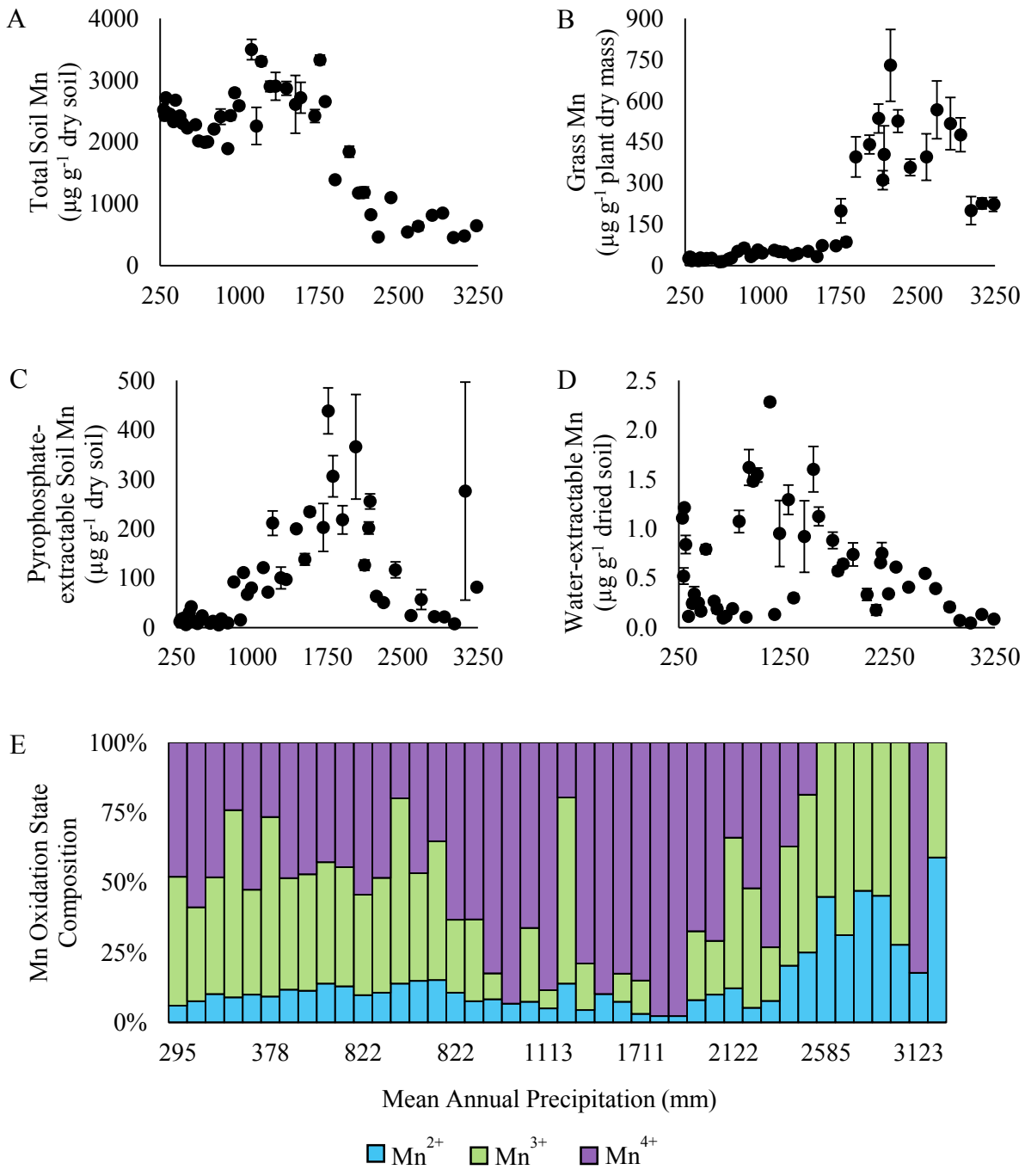
A
Total Soil Mn (µg g-1 dry soil)
4000
3000
2000
1000
0
250
1000
1750
2500
3250
B
Grass Mn (µg g-1 plant dry mass)
900
750
600
450
300
150
0
250
1000
1750
2500
3250
C
Pyrophosphate-extractable Soil Mn (µg g-1 dry soil)
500
400
300
200
100
0
250
1000
1750
2500
3250
D
Water-extractable Mn (µg g-1 dried soil)
2.5
2.0
1.5
1.0
0.5
0.0
250
1250
2250
3250
E
Mn Oxidation State Composition
100%
75%
50%
25%
0%
295
378
822
822
1113
1711
2122
2585
3123
Mean Annual Precipitation (mm)
Mn2+
Mn3+
Mn4+

Figure 2.

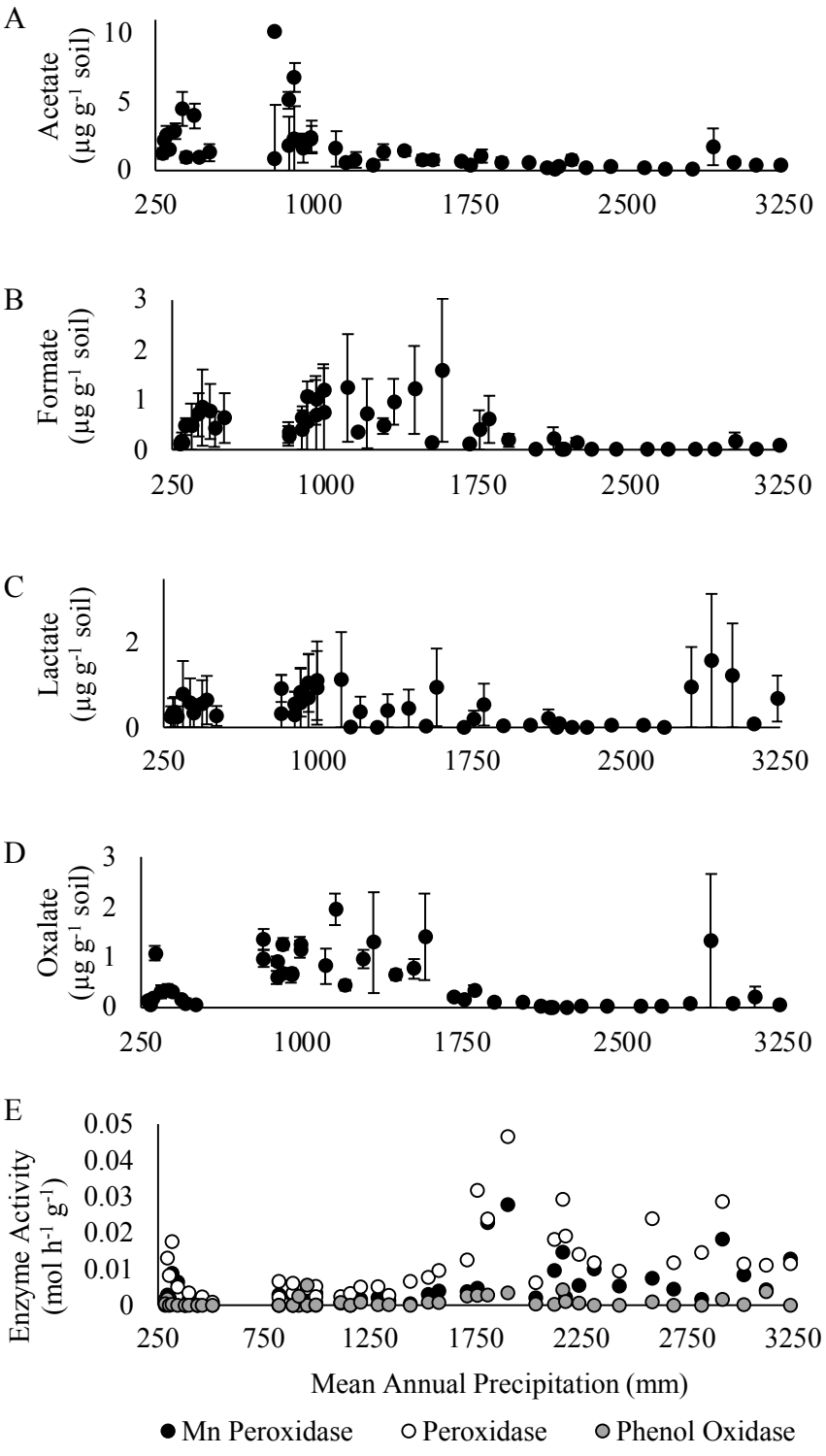
A
Acetate (µg g-1 soil)
10
5
0
250
1000
1750
2500
3250
B
Formate (µg g-1 soil)
3
2
1
0
250
1000
1750
2500
3250
C
Lactate (µg g-1 soil)
2
0
250
1000
1750
2500
3250
D
Oxalate (µg g-1 soil)
3
2
1
0
250
1000
1750
2500
3250
E
Enzyme Activity (mol h-1 g-1)
0.05
0.04
0.03
0.02
0.01
0
250
750
1250
1750
2250
2750
3250
Mean Annual Precipitation (mm)
Mn Peroxidase
Peroxidase
Phenol Oxidase

Figure 3.

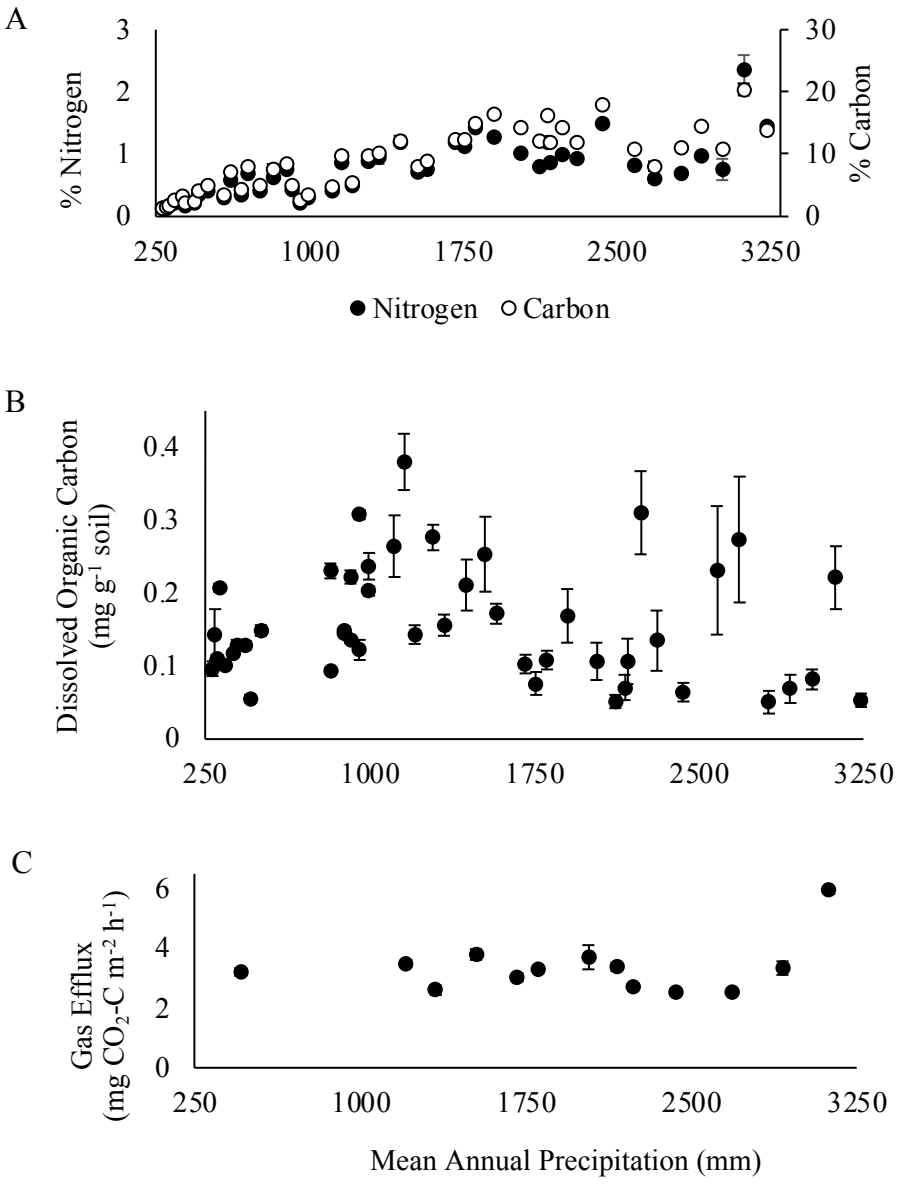

Figure 4.

1136

1137

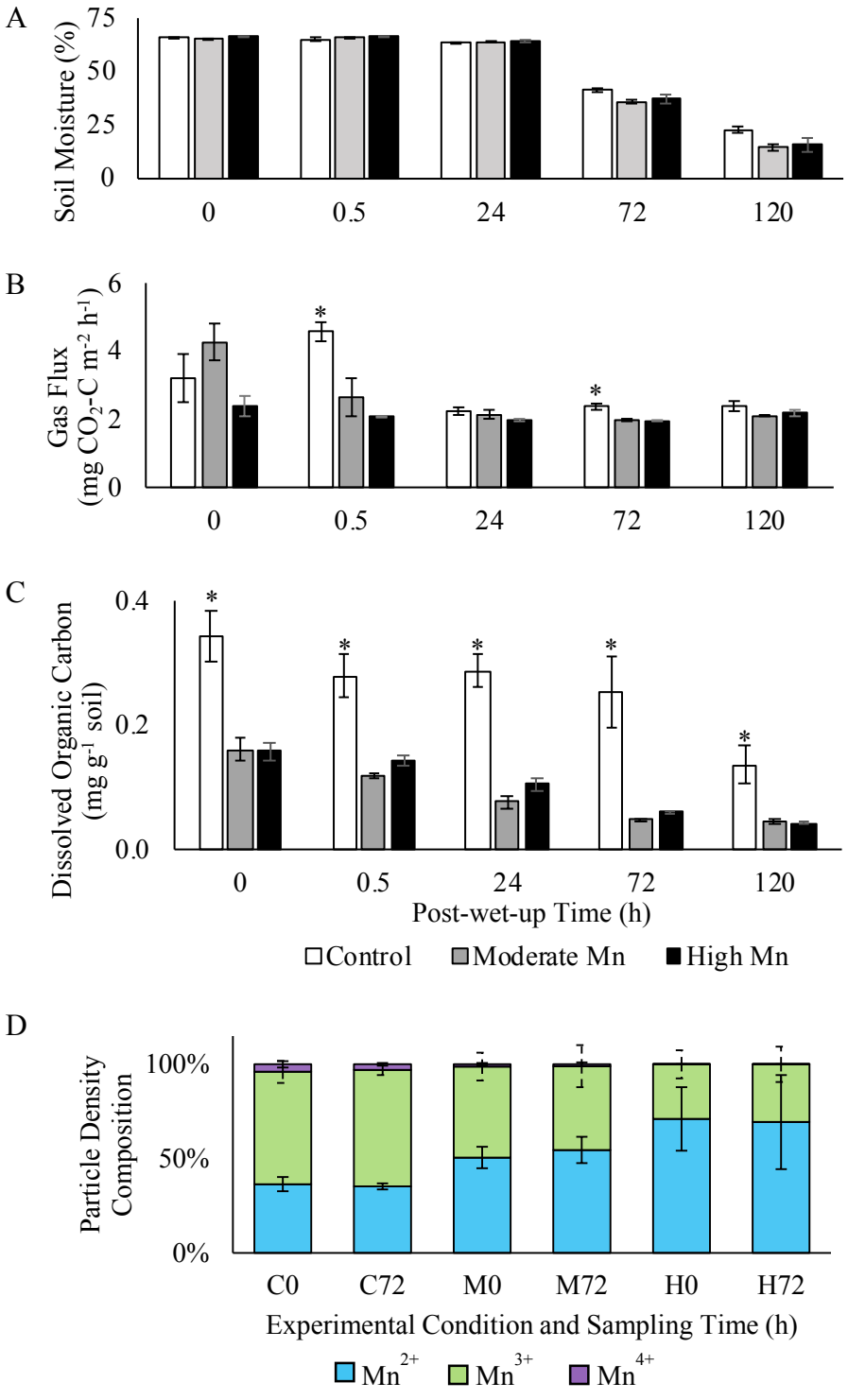

Figure 5.

1138

10. Supplementary Information: Methods

10.1 Soil pH

Soil pH (Figure S1A) was measured in samples collected from each site in the summers of 2019 and 2021. Soil samples were mixed with deionized (DI) water in 1g:1mL slurries and shaken for 5 min (Thomas, 1996). Slurries stood for 10 min before pH was read. Each soil sample was measured six times.

10.2 Soil Redox-potential (Eh) and Temperature Measurements

Platinum (Pt) electrodes and reference probes were designed to minimize soil disturbance and to maximize field durability and measurement reproducibility. Pt-electrodes were constructed as described in Wanzek et al. 2018 (Wanzek et al., 2018). Accordingly, 1.5-cm lengths of 16-gauge 99.9% pure Pt wire (American Elements, Los Angeles, CA USA) were soldered using lead-free silver solder wire (Oatey Co., Cleveland, OH USA) to 0.5-m lengths of insulated 16-gauge copper wire (Cerrowire, Hartselle, AL USA); soldered junctions were reinforced with heat-shrink tubing (Gardner Bender, Milwaukee, WI USA). Pt-Cu wires were fed into plastic 10-mL pipette tips (Rainin RC UNV 10mL 200A/1, Mettler-Toledo, Oakland, CA USA), exposing 1 cm of the Pt-wire through the pipette tips tapered end and sealed in place with epoxy.

Silver-silver chloride (Ag-AgCl) reference electrodes were constructed according to Barlag et al. 2014 (Barlag et al., 2014, p. 201). Accordingly, five 1-cm-diameter holes were drilled into 15-mL centrifuge tubes (Corning, Corning, NY USA): one hole through the center of the tapered tip, three holes around the tube's circumference 2 cm from the end, and one hole in the cap; holes at the bottom of the centrifuge tubes allow the salt bridge to contact the soil, and the hole in the cap allows the Ag-AgCl to exit the capped tube and connect to the voltmeter. The tubes

were then acid-washed, rinsed in deionized (DI) water, dried, and placed upright and uncapped in a 500-mL beaker. The agarose-gel salt bridge was prepared by dissolving 7 g of lab-grade agarose and 25 g of potassium nitrate (KNO_3) in 500 mL of heated DI water. The heated solution was poured into the beaker containing the prepared centrifuge tubes to a depth sufficient to fill the tubes with 5 mL of solution. The agar solution was left to cool and harden in the tubes for 24 h; the tubes were then stored at 4°C until needed for field use.

AgCl(s) was chemically deposited onto Ag(s) by immersing 8-cm segments of 18-gauge 99.9% pure Ag wire (Rio Grande, Albuquerque, NM USA) in laundry bleach (Clorox, Oakland, CA USA) for 30 min at 25°C. The wires were removed, rinsed in DI water, and stored at 25°C in a foil-covered container filled with potassium chloride (3M KCl). Pt-electrodes and reference electrodes were tested for accuracy prior to installation in the field using commercial redox/ORP standards (Orion, Thermo Scientific, Waltham, MA USA). If any probe deviated more than +/- 10 mV outside of the standard reference potential at 25°C (220 mV), the Pt-electrode was cleaned, the batch of reference probes was thrown out and remade, and the probes were retested (Jones, 1966; Austin and Huddleston, 1999; Thermo Fisher, 2007).

In September 2021, soil redox potential (E_h) and surface temperature were measured using a Fluke 289 True-RMS Data Logging Multimeter (Everett, WA USA) and hand-held manual digital thermometer (Garmin, Olathe, KS USA) in 13 sites along the Kohala rainfall gradient. Soil surface temperature was manually measured every minute for 10 min before and after electrodes were installed; measurements were averaged over the 20-min collection period for each site. Pt- and reference electrodes were seated 3-cm deep in soil; this consistent depth was used after deeper placement in the dry sites was found to substantially alter the soil structure and/or damage the probes. Once in place, reference electrodes were filled with 3M KCl and Ag-AgCl wires were

inserted into the tubes through the drilled holes 1 cm below the tube caps, leaving 1-cm wire segments outside of the 3M-KCl-filled centrifuge tubes to connect to the voltmeter. A plastic toolbox was used to protect the electrodes and multimeter from strong winds, sun exposure, rainfall, and animals: two holes were drilled in the bottom of the toolbox to allow the electrodes to sit in the soil, and the toolbox was latched closed and tethered in place. Redox potential measurements were automatically logged every 10 min for 25 h: 12 h at the start of data collection were discarded to allow electrodes time to equilibrate *in situ*; the final hour of data collection was also neglected to provide a buffer between data collection and instrument retrieval; data from the remaining 12 h (n = 73 timepoints) were normalized relative to the standard hydrogen electrode, calculated using daily soil temperature data for each site (Nordstrom and Wilde, 2005; Wolkersdorfer, 2008). Data are shown in Figure S1C.

11. Supplementary Tables

Table S1. Background characteristics for the site on the Kohala rainfall gradient where soil for the experiment was collected. 10-cm soil cores were collected, manually homogenized, and cleaned of plant, rock, and fauna material. All reported values are means, n=3–6 replicates. Standard error of the mean = SEM. Mean Annual Precipitation (MAP) is ~2163 mm (Giambelluca et al. 2013). Soils were collected in the summers of 2018, 2019, and 2021.

Soil Feature	Mean	SEM
Volumetric Water Content (θ)	0.440	0.0300
pH	4.47	0.0200
total soil manganese (Mn) (μg g^{-1} dried soil)	1180	17.8
plant-available Mn (μg g^{-1} dried plant mass)	311	34.6
deionized (DI) water extractable Mn (μg g^{-1} dried soil)	0.658	0.0290
extractable (organically bound) Mn (μg g^{-1} dried soil)	201	12.2
% Carbon	16.1	0.280
% Nitrogen	1.19	0.0500
dissolved organic carbon (DOC) (mg g^{-1} soil)	0.0700	0.0170
CO_2 flux per unit area (mg CO_2-C m^{-2} h^{-1})	3.38	0.140
Mn peroxidase (MnP) activity (μmol h^{-1} g^{-1} soil)	14.9	NA
peroxidase activity (μmol h^{-1} g^{-1} soil)	29.2	NA
phenol oxidase activity (μmol h^{-1} g^{-1} soil)	4.26	NA

Mn compositions collected using X-ray absorption near-edge structure (XANES) spectroscopy on single replicates of homogenized 10-cm soil samples.

Mn Oxidation State	Composition (%)
Mn^{2+}	5.30
Mn^{3+}	42.6
Mn^{4+}	52.1

12. Supplementary Figures

Figure S1. A) Soil pH and B) Volumetric Water Content (VWC, Θ) measured in homogenized 10-cm soil cores along the gradient. Filled markers represent averaged values (n=3–6). Error bars illustrate the standard error of the mean (SEM). C) Standard reduction potentials measured to 3-cm soil depths in sites with sufficient soil moisture (receiving ≥ 1750 mm MAP) along the gradient. Filled markers symbolize average standard reduction potentials taken every 10 minutes for 10 hours. Error bars represent standard deviations (SD). D) Contribution of manganese (Mn) peroxidase (MnP) activity to ligninolytic enzyme activity, expressed as percent MnP activity of the summed enzyme activity for each gradient site. Filled markers represent % MnP of total enzyme activity. Average percentage is 28.5%, median is 28.4%, and maxima are 55.9% at 343 mm mean annual precipitation (MAP) and 52.5% at 3238 mm MAP.

Figure S2. Representative manganese (Mn) X-ray absorption near-edge structure (XANES) spectra and their corresponding fits of gradient soil; homogenized 10-cm soil cores were collected from each gradient site. The measured Mn K-edge XANES spectra are shown in black; principal component analysis (PCA) and linear combination fitting (LCF) were used to determine Mn^{2+}, Mn^{3+}, and Mn^{4+} peaks; LCF fits are shown in red. Vertical dashed lines indicate the approximate positions of Mn^{2+}, Mn^{3+}, and Mn^{4+} peaks across spectra. Numbers to the right of spectra identify the mean annual precipitation (MAP) (mm) of site samples.

Figure S3. A) Open mason jars and lids with compression fittings to measure soil CO_2 flux from field soils. B) Sealed mason jars with equal volumes of soils. Soils were manually homogenized, picked through to remove root matter and rocks, and transferred to mason jars within hours of

field collection. Soils rested in open mason jars for 24 hours before we capped the jars and started CO_2 collection. C) The experimental array of mason jars for gas and soil sampling is shown. B) The compression fitting through the mason jar lid, shown from D) above and E) side, allow for gas sampling from the air-tight, sealed jar. The jars remained open (unlidded) between sampling timepoints.

Figure S4. Images of thin-sectioned soils collected from each condition at Time 0 and 72 hours. Images were created using μ-X-ray fluorescence (XRF) analyses at SLAC SSRL: A) Control at hour 0, B) Control at hour 72, C) Moderate Manganese (Mn) at hour 0, D) Moderate Mn at hour 72, E) High Mn at hour 0, and F) High Mn at hour 72. The distribution of Mn oxidation state Mn^{2+} is represented by blue, Mn^{3+} by green, and Mn^{4+} by red.

Figure S5. A) Composition of manganese (Mn) oxidation states in deionized-water (DIW) and sodium-pyrophosphate (NaPP) extracts of homogenized 10-cm soil cores collected along the Kohala rainfall gradient. Blue columns symbolize the percentage of Mn^{2+}, green columns Mn^{3+}, and purple columns Mn^{4+}. Mn oxidation states were identified and assigned using X-ray absorption near-edge structure (XANES) spectroscopy, principal component analysis (PCA), and linear combination fitting (LCF). B) XANES spectra and fits: black lines represent measured spectra, and red lines represent fits based on PCA and LCF analyses.

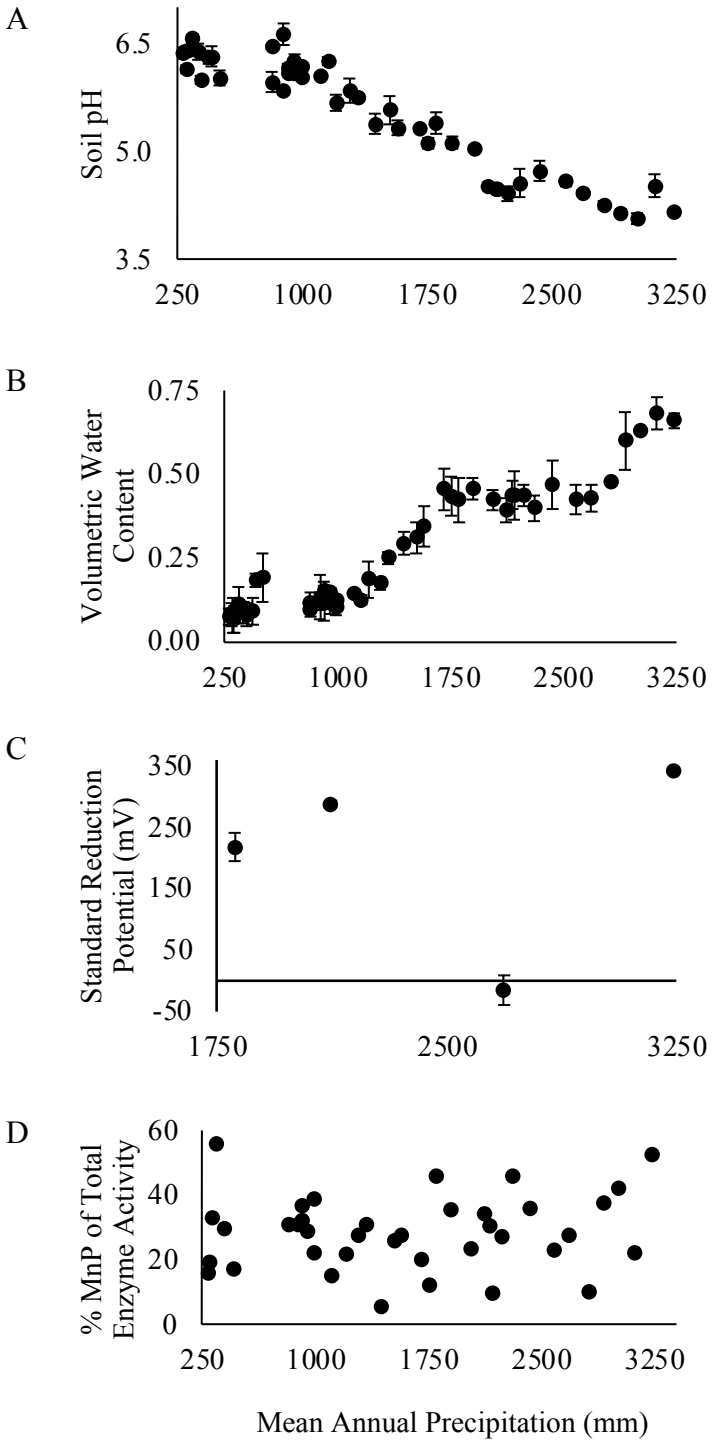

1243

Figure S1.

1244

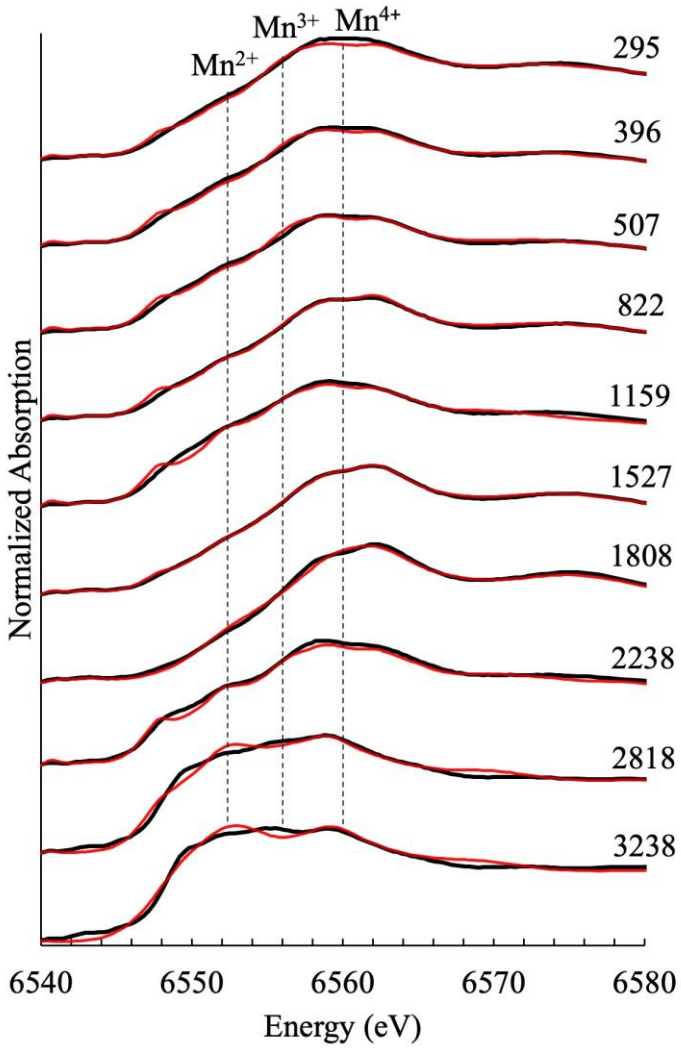
Mn3+
Mn4+
Mn2+
295
396
507
822
1159
1527
1808
2238
2818
3238
Normalized Absorption
6540
6550
6560
6570
6580
Energy (eV)

Figure S2.

Figure S3.

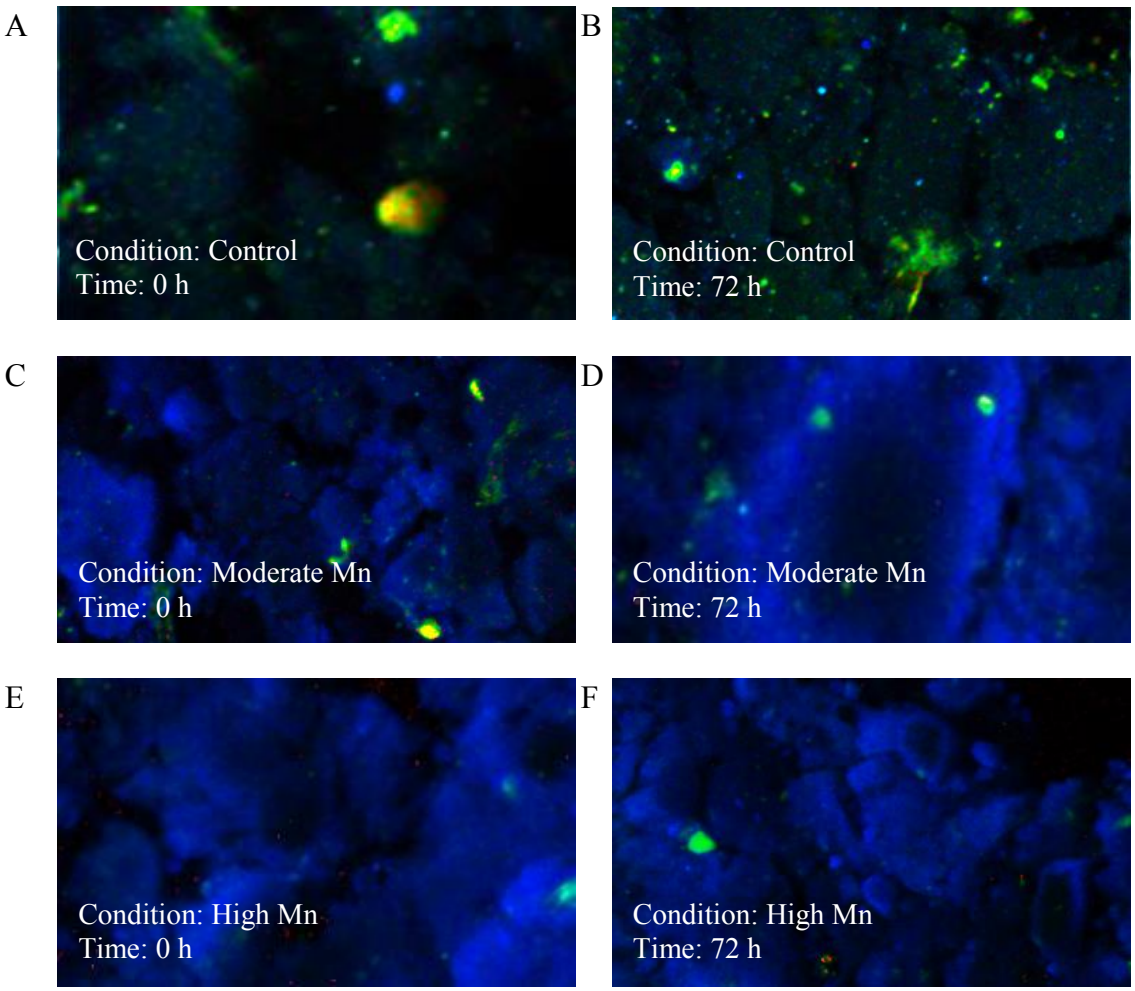

1249

Figure S4.

1250

A

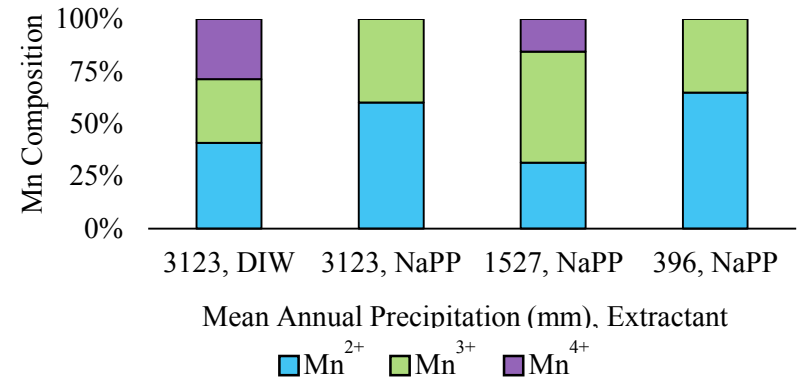

B

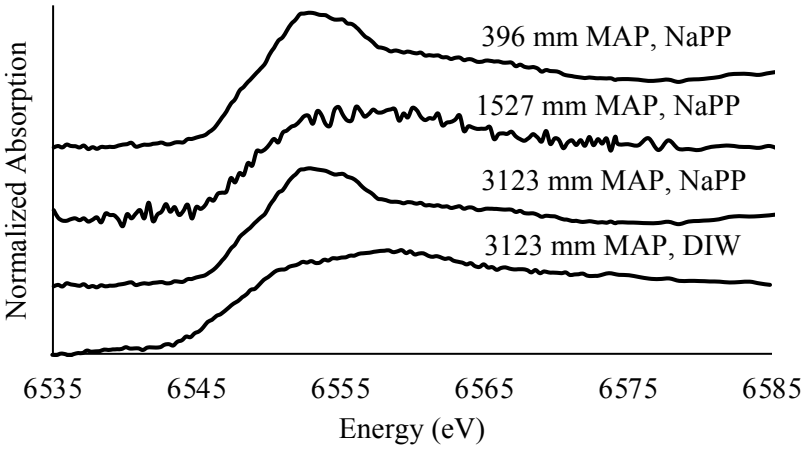

Figure S5.

1251